ELSEVIER

Contents lists available at ScienceDirect

Ore Geology Reviews

journal homepage: www.elsevier.com/locate/oregeorev





Evolution of the gold (copper) mineralization in the porphyry stock and the related skarn zones and epithermal veins in the Astarghan area, NW Iran: Evidence from fluid inclusion, mineral chemistry and sulfur isotope analyses

Rasoul Ferdowsi*, Ali Asghar Calagari, Vartan Simmonds, Azinsadat Miranvari

Earth Sciences Department, Faculty of Natural Sciences, University of Tabriz, 5166616471 Tabriz, Iran

ARTICLE INFO

Keywords: Astarghan Porphyry mineralization Epithermal gold Fluid inclusion S isotope EPMA

ABSTRACT

The Astarghan area in northwest Iran (~50 km north of Tabriz) represents an excellent example of coexisting and associated skarn, porphyry and epithermal mineralizations of copper and gold. This contribution aims to study the geology, alteration and mineralization in these deposits, as well as the occurrence of gold and its host minerals, and present the physico-chemical characteristics of ore-forming fluids and the sulfur origin, in order to get a better understanding of development and evolution of these mineralizations. The Astarghan porphyry stock (Oligo-Miocene) intruded the upper Cretaceous flysch-type sedimentary sequence (calcareous sandstone and limestone with intercalations of siltstone, shale and marl) and brought about metamorphism and metasomatism along the contact. The Cu-Au mineralization in the Astarghan area occurred mainly in three forms: (1) skarn patches along the contact (Zone A), (2) stockwork-type and disseminated porphyry mineralization within the potassic (at Kaghdara and Boiokwari areas) and phyllic (at Sildirimdara area) alteration zones (Zone B), and (3) native gold-bearing low-sulfidation epithermal veins within the argillic alteration zone at Nowrozkala area (Zone C). The micro-thermometric studies on the porphyry-type Kaghdara potassic alteration zone showed that homogenization temperatures for liquid-rich and vapor-rich 2-phase, as well as halite-bearing multiphase inclusions range about 160-420 °C, 220-460 °C, and 320-580 °C, respectively. Salinities of the 2-phase and multiphase inclusions have ranges of 5-25 and 40-70 wt% NaCleq., respectively. However, fluid inclusions present in the epithermal veins of Nowrozkala are mainly liquid-rich 2-phase, and their homogenization temperature and salinity values lie within the ranges of $118-325~^{\circ}C$ and 0.6-7.4 wt% NaCl_{eq.}, respectively. The approximate estimated depth of the sulfide and gold mineralization in the porphyry system ranges from 1.6 to 2.5 km, and in the epithermal system is < 0.9 km. The sulfur isotopic analysis of pyrite from the porphyry and epithermal mineralizations in the potassic alteration zone at Kaghdara and argillic alteration zone at Nowrozkala indicate that the δ^{34} S values (-0.1 to -0.3 and -0.5 to -1.1\,\(\text{w}\), respectively) are close to the range of magmatic sources. Finally, electron probe micro-analyses indicate that besides independent particles of 50-200 µm in the epithermal veins, gold is mainly hosted by tetrahedrite within the porphyry-related phyllic alteration zone, but especially stibnite within the epithermal veins; these minerals, as well as epithermal polyhedral pyrites contain native gold inclusions.

1. Introduction

Mineral deposits of the porphyry–epithermal system are generally associated with magmatic arcs in convergent geodynamic settings and display spatial and temporal relationship with intermediate to felsic subvolcanic intrusions (Seedorff et al., 2005; Simmons et al., 2005). In all

cases, these deposits are thought to have formed at shallow crustal levels ($<1.5~\rm km$ for epithermal and $<6~\rm km$ for porphyry deposits [Seedorff et al., 2005; Simmons et al., 2005]). One of the most significant metallogenic belts hosting large metallic mineral resources of these types is the Alpine–Himalayan metallogenic belt, extending from Eastern Europe through Central Asia to the Pacific region, which was formed as

E-mail address: Ferdowsirasol@gmail.com (R. Ferdowsi).

^{*} Corresponding author.

the result of a very complex tectonic evolution during the history of Paleo- and Neo-Tethys oceans, involving subduction of the oceanic crust. Thus, various types of mineralization are related to a variety of tectonic settings such as intracontinental rifting, ocean-floor spreading, subduction-related rifting, and continent-continent collision (Singer et al., 2005; Richards, 2015).

The middle section of this belt passes through the Iranian territory, represented by the Alborz and Zagros mountain ranges. Therefore, Iran documents the closure of at least two Tethyan oceans, (1) Paleo-Tethys during the Paleozoic and (2) Neo-Tethys during the Cenozoic (Sengör and Natal'in, 1996; Richards et al., 2006; Richards, 2015). Although a

small number of mineral deposits and the related igneous rocks are associated with the Paleo-Tethys ocean in Iran (e.g., early Cambrian Kiruna-type iron oxide–apatite deposits in the Bafq area of Central Iran), it is the Cenozoic Urumieh–Dokhtar magmatic arc (UDMA) that played a significant role in the formation and distribution of many porphyry–epithermal deposits throughout Iran (Fig. 1a). This arc is over 2000 km long and ~ 50 km wide and is associated with the Late Meso-zoic–Early Cenozoic northeastward subduction of the Neo-Tethyan oceanic crust beneath the Central Iranian plate, as a result of collision of the African and Eurasian plates (Alavi, 1994; Stampfli, 2000; Omrani et al., 2008). The UDMA also coincides with the porphyry copper

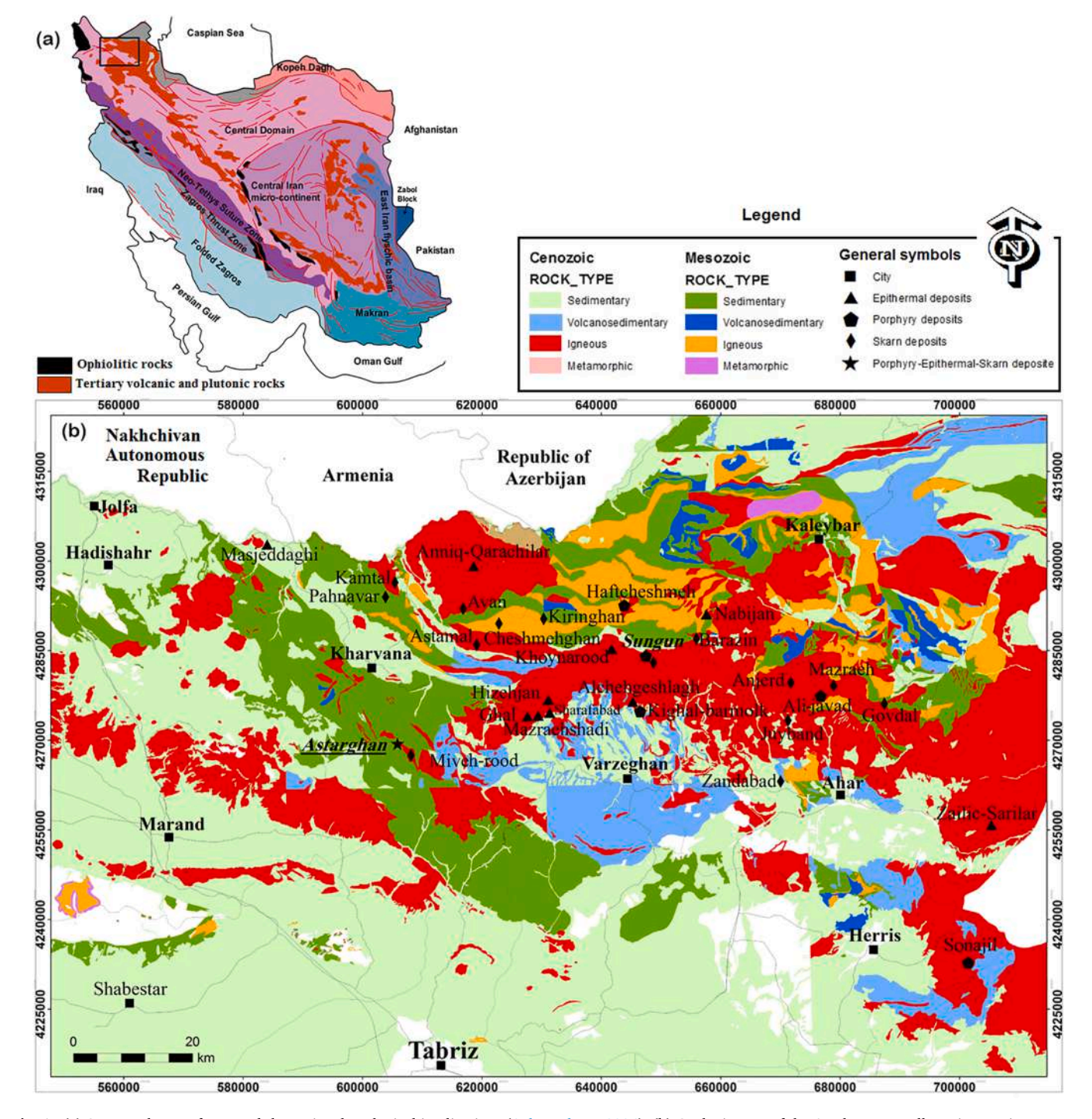


Fig. 1. (a) Structural map of Iran and the regional geological implications (Agha Nabaty, 2004). (b) Geologic map of the Arasbaran metallogenic zone in NW Iran, showing the distribution of Mesozoic and Cenozoic magmatic rocks and the associated porphyry, epithermal and skarn deposits.

metallogenic belt of Iran, which is in turn divided into three main metallogenic zones located in the northwest (Arasbaran zone), center, and southeast (Kerman zone) of the arc (Ghorbani, 2013). The most prosperous zone is the Kerman zone, where is located the nation's largest porphyry copper deposit (PCD) (Sarcheshmeh [Shahbpour, 1982], as well as Miduk [Taghipour et al., 2008], Sarkuh and Iju [Mirnejad et al., 2013] and many other large and small deposits and prospects). The central metallogenic zone for Cu is represented by PCDs such as Dalli [Ayati et al., 2013; Fatehi and Asadi, 2017; 2019] and Kahang [Komeili et al., 2017]), as well as epithermal deposits such as Shanegh (Sakhdari et al., 2011). Some porphyry and epithermal deposits also occur in East Iran (e.g., Shadan [Richards et al., 2012] and Sharaf Abad [Karimpour et al., 2011] PCDs and Chah Shalghami epithermal deposit [Karimpour et al., 2011]).

The northwestern part of the UDMA is known as the Arasbaran or Ahar-Jolfa metallogenic zone, which extends from south Armenia to the northwest of Iran, and is regarded as part of the lesser Caucasus in the Alpine-Himalayan metallogenic belt. The Cenozoic magmatism and accompanying porphyry–skarn–epithermal mineralizations in this zone were the result of post-collisional, slab breakoff-induced heat and fluid flow from upwelling asthenosphere beneath the young orogenic belt (Jamali et al., 2010; Simmonds, 2013). Both $Cu \pm Mo$ and $Cu \pm Au$ porphyry and epithermal types of deposits of Late Eocene, Middle Oligocene and Early Miocene exist in the Arasbaran zone, mainly associated with the emplacement of Middle Eocene to Miocene magmatic pulses in the Qaradagh batholith and the Shaivar-Dagh plutonic complex, as well as numerous satellite stocks within the Cretaceous-Cenozoic sedimentary-volcanic sequence (e.g., Aghazadeh et al., 2011; Ghorbani, 2013). Some of these well-known deposits are the porphyry Cu-Mo deposits at Sungun (Calagari, 2003; 2004a; 2004b; Aghazadeh et al., 2015; Simmonds et al., 2017), Haft-Cheshmeh (Aghazadeh et al., 2015), Kighal (Simmonds, 2013; 2019; Simmonds et al., 2015), Ali-Javad (Hajalilou and Aghazadeh, 2016), Sonajil (Hosseinzadeh et al., 2010), vein-type and possible porphyry Cu-Mo mineralization at Qarachilar (Simmonds and Moazzen, 2015; Simmonds et al., 2016), porphyry Cu-Au mineralization in the Mirkuh Ali Mirza deposit (Maghsoudi et al., 2014), the Masjed Daghi Cu-Au porphyry-epithermal mineralization (Atalou et al., 2017), the epithermal gold deposits of Mazraeh-Shadi (Radmard et al., 2017), Nabijan (e.g., Jamali et al., 2017), Zailic-Sarilar (Miranvari et al., 2020), and finally the Cu-Fe skarns of Mazraeh (Mollai et al., 2009) and Sungun (Calagari and Hosseinzadeh, 2006) (Fig. 1b).

Also, various types of mineralization were formed within the northward extension of the Qaradagh batholith in South Armenian Block (Meghri–Ordubad pluton) including the Agarak, Kadjaran (Zvezdov et al., 1993; Moritz et al., 2016a; 2016b; Rezeau et al., 2016) and Paragachay (Babazadeh et al., 1990; Moritz et al., 2016a) porphyry Cu–Mo deposits, Zod epithermal gold deposit (Konstantinov et al., 2010; Moritz et al., 2016a), and the Kapan, Alaverdi and Mehmana deposits with a hybrid VMS–epithermal–porphyry genesis (Mederer et al., 2014; Moritz et al., 2016a).

The Astarghan deposit also lies on the UDMA belt at NW Iran, where skarn, porphyry and epithermal mineralizations of Cu and Au have occurred consecutively. As a result, studying this mineral deposit may elucidate the evolution of magmatic–hydrothermal ore-forming fluids upon emplacement of the intrusive body and formation of contact metamorphism and metasomatites, through hydro–fracturing and generation of porphyry-type stockwork and disseminated mineralization, up until the occurrence of epithermal mineralization. In this regard, the present research focuses mainly on the geology, alteration, mineralization and fluid characteristics, including temperature, salinity and sulfur origin, in order to get a better understanding of the development and evolution of the deposits, as well as to identify the occurrence of gold and its host minerals.

2. Geology of the Astarghan area

The Astarghan area, part of the UDMA and the Arasbaran metallogenic zone, is located $\sim 50~\rm km$ north of Tabriz. As shown by the geologic map of Fig. 2, the upper Cretaceous to Paleocene flysch-type rocks, comprised of calcareous sandstone and limestone with intercalations of siltstone, shale and marl, are the prevalent units in the Astarghan area. These units have been folded by the Pyrnean orogenic phase, resulted in the formation of many synclines and anticlines with general trend of N130E, along with faults and fractures.

The Astarghan sub-volcanic porphyry stock (granodiorite to quartz-monzonite in composition) intruded the upper Cretaceous–Paleocene sequence. Based on the stratigraphic relationships and the presence of similar dated intrusives in neighboring areas, its age can be attributed to Oligo–Miocene (Regional Company of Azarbaidjan Mines, 1995). Its main surficial outcrops are found at Kaghdara, Sildirimdara and Nowrozkala (Fig. 2).

The flysch sequence was thermally metamorphosed following the emplacement of the Astarghan stock, and resulted in the development of skarn patches, hornfels and marble (Fig. 3a). The major skarn patches crop out mainly at Kaghdara (Zone A). Volcanic rocks comprised of andesitic and trachytic lavas and tuffs have intimate relationship with intrusive rocks and probably represent their igneous equivalents. They are mainly seen at topographic heights of the area (e.g., at Nowrozkala) and show the impacts of tectonic activities in the form of numerous joints and fractures. Two dike generations (1-40 m thick) cut the stock, metasomatites and sedimentary rocks, which have been characterized by their composition, mineral assemblage and their general trend. The first generation is of granodioritic composition with NW-SE trend, while the second has a monzodioritic to microdioritic composition with mainly NE-SW trend and cross-cut the first generation (Fig. 3b). There are also surficial outcrops of monzodioritic and andesitic sills (Fig. 3c), which have considerable lengths up to 10 km and display weak marginal metamorphic haloes. Limited outcrops of Pliocene limestones are found to the south and southeast of the Astarghan village, which unconformably overlie the flysch-type units. Finally, Quaternary elluvial deposits, alluviums and terraces are the youngest units in the study area.

3. Materials and methods

Field work was carried out in the spring of 2013, aiming to determine the rock types, hydrothermal alterations and mineralization zones. Over 200 representative samples were collected from magmatic, metasomatic and sedimentary rocks, alteration zones and mineralized veins/veinlets. Laboratory studies included examination of 50 thin-polished sections at the University of Tabriz. In order to identify unrecognizable mineral phases, 15 rock samples were also analyzed by XRD (Philips-Xpert Pro model) at the Iranian Mineral Processing Research Center (IMPRC) in Karaj. In order to determine the main oxides and major, minor and trace elements, 12 fresh rock samples from the porphyry stock were chemically analyzed by XRF (Philips-Magix pro), ICP-OES (Agilent 730 model) at IMPRC and ICP-MS (Agilent 7900 model) techniques in ACME Labs (Canada).

Fluid inclusion studies were performed on 20 doubly polished quartz sections (~100 μm thick) collected from veins/veinlets of surficial outcrops and diamond drill cores, of which 15 sections from garnets in the skarn zone, veins/veinlets within the porphyry-type potassic alteration zone at Kaghdara and phyllic alteration zone at Sildirimdara (145 fluid inclusions), as well as epithermal veins/veinlets at Nowrozkala (103 fluid inclusions) were subjected to micro-thermometric analysis at IMPRC, using a Linkam THMS600 heating–freezing stage installed on a ZEISS microscope. The thermal range of the device was from –196 °C to + 600 °C. The measurement precision on heating and freezing stages was \pm 0.6 °C and \pm 0.2 °C, respectively. The results are presented in Table 1.

Sulfur isotopic analysis was performed on four pyrite separates,

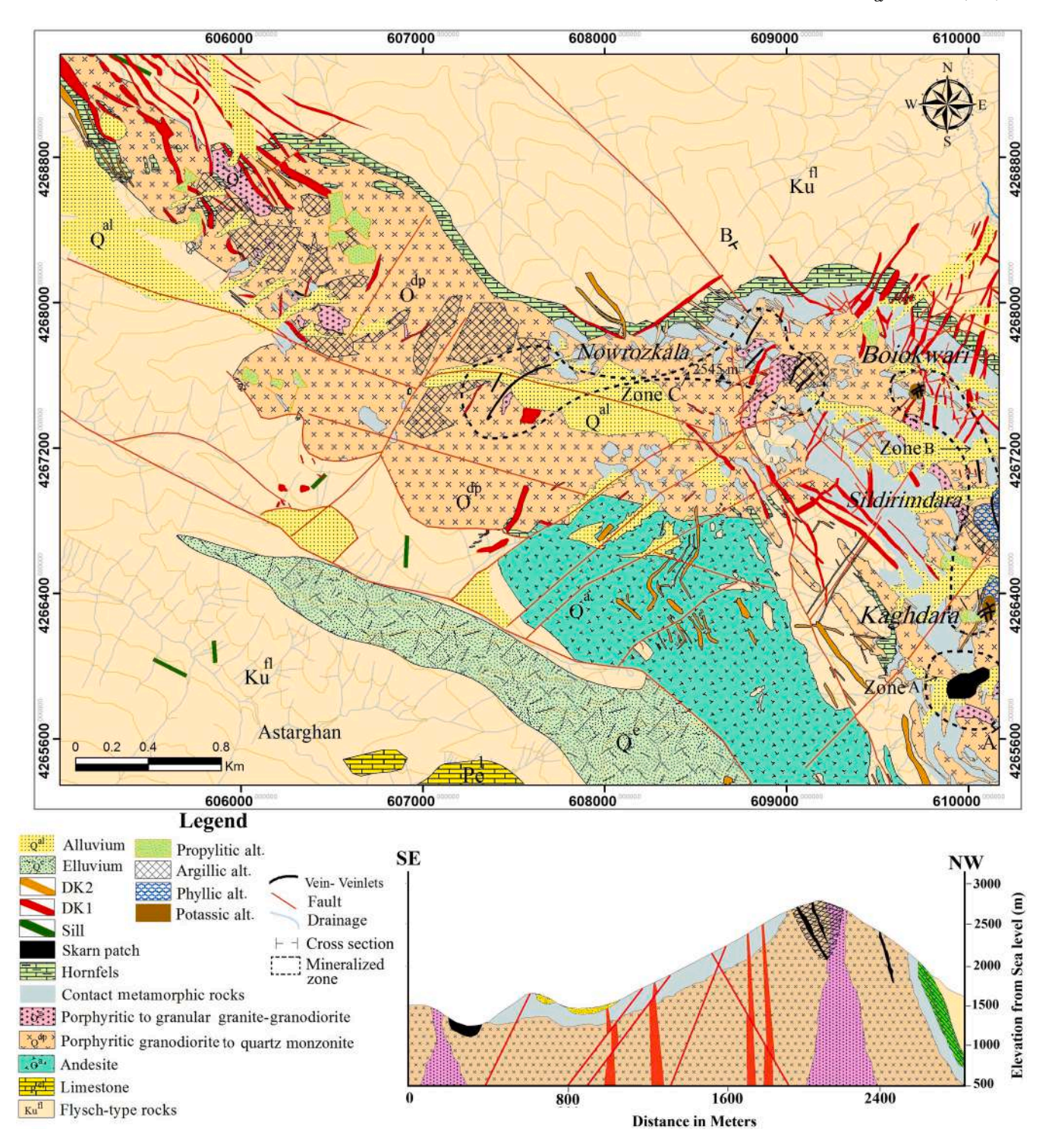


Fig. 2. Geologic map of the study area (with modifications after the Regional Company of Azarbaidjan Mines, 1995) and a cross section along A–B direction. Shown in this map are also the positions of three major mineralized zones (Zones A, B, and C).

collected from Au-bearing quartz veins/veinlets of the porphyry (n = 2) and epithermal (n = 2) mineralizations within the porphyry stock, due to its intimate relationship with gold, larger crystal size and appearing as the only purely separable sulfide phase from the veins/veinlets (Table 2). Determination of $\delta^{34}S_{CDT}$ was performed at the Stable Isotope Laboratory of Salamanca University (Spain). The procedures for the combustion of the samples followed the method of Robinson and Kusakabe (1975). The $^{34}S/^{32}S$ isotope ratio was measured by spectroscopic methods on SO_2 obtained in a high vacuum line by combustion in a tubular furnace at 1070 °C. Isotopic ratios were measured in a VG

Isotech SIRA-II mass spectrometer. Sulfur isotope composition is expressed in delta per mil notation with respect to the Canyon Diablo Troilite (CDT) standard. The estimated analytical error, determined by repeated analyses of international and internal standards was better than $\pm~0.2\%$.

The accurate chemical composition of the minerals (sulfides and sulfosalts) and their gold contents were determined by Electron-probe microanalysis (EPMA) (Cameca, SX100) at IMPRC. In this regard, 8 polished sections (3 from the host intrusive body and 5 from the ore-bearing veins/veinlets), including 160 points on metallic and non-

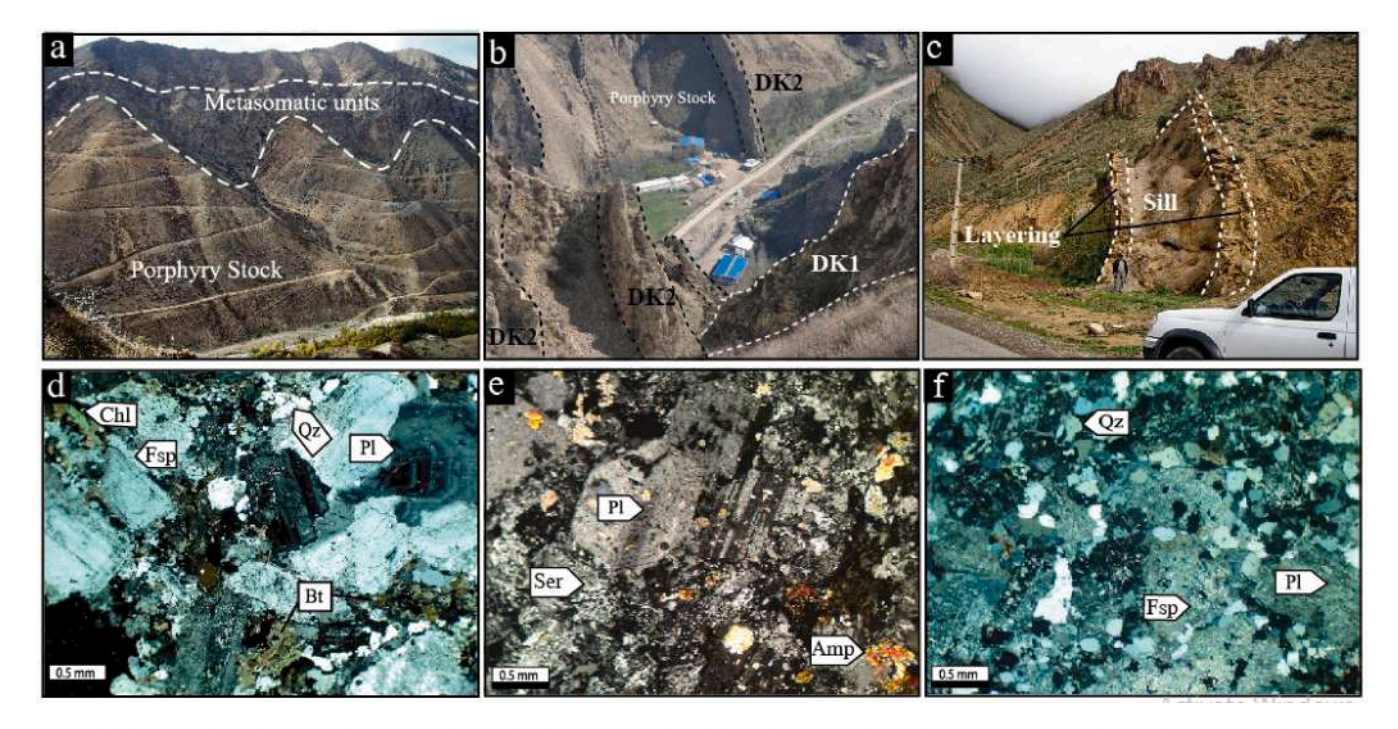


Fig. 3. Field photographs of the surficial outcrops along with photomicrographs of the rock types in the study area. Outcrops of the porphyry stock and metasomatic rocks along the contact (view towards NW). (b) Two generations of dike swarms with NW–SE and NE–SW trends in the study area (view towards NE). (c) Outcrop of a sill following the bedding plane of the sedimentary rocks (view towards N). (d) Plagioclase, K-feldspar, biotite and quartz showing granular texture within the granodioritic porphyry stock (XPL). (e) Plagioclase and amphibole within the granodioritic dike (XPL). (f) Plagioclase, quartz and chlorite within a sill (XPL). Mineral abbreviations are from Whitney and Evans (2010).

Table 1 Summary of microthermometric data from fluid inclusions (all temperature are in °C, and salinities are expressed as wt% NaCl_{eq.}); L = liquid, V = vapor, H = halite, S = solid, P = primary.

Mineralization type	Inclusion type	Size (µm)	Origin	Tm ice (°C)	T _{S(NaCl)} (°C)	$T_{H(L-V)}$ (°C)	Mode	Salinity
Porphyry (potassic zone)	LV (n = 36)	7–21	P	−3 to −20.3	-		$L + V \rightarrow L$	5.0-23.3
	VL (n = 14)	15-25	P	-4.5 to -21.8	-	168-418	$V + L \rightarrow V$	7.0-22.6
	LVH $(n = 60)$	6–15	P		300-568	228-460	$L+V+H\to L$	40.3-69.3
	LVH + S? (n = 4)	12	P		400-540	320-568	$L+V+H+S \rightarrow V$	27.7-65.3
						212–520		
Porphyry (phyllic zone)	LV(n = 31)	6–30	P	−3 to −4.9	_	175–345	$L + V \rightarrow L$	5.1-8.0
Epithermal (argillic zone)	LV $(n = 103)$	5–23	P	-0.5 to -4.6	_	118–325	$L+V\toL$	0.6–7.4

 Table 2

 Sulfur isotopic composition of pyrite samples from the study area.

Mineralization type	Location	Mineral	δ ³⁴ S (‰)	δ ³⁴ S H ₂ S (‰)
Porphyry	Qtz. stockwork	Pyrite	-0.1	-0.7
	Qtz. stockwork	Pyrite	-0.3	-1.1
Epithermal	Qtz. vein	Pyrite	-0.5	-2.1
	Qtz. vein	Pyrite	-1.1	-2.7

metallic minerals from skarn, porphyry and epithermal systems were subjected to EPMA, and the results are shown in Table 3.

4. Results

4.1. Petrography of the Astarghan porphyry stock, the cross-cutting dikes and sills

Based on petrographic studies, the Astarghan porphyry stock consists of plagioclase, quartz, amphibole, biotite, alkali feldspar and clinopyroxene (Fig. 3d), ranging in composition from granodiorite to quartzmonzonite. Plagioclase (45–60 vol%) occurs as phenocrysts (0.5–2

mm), portraying polysynthetic twinning and oscillatory zoning. K-feld-spar (15–20 vol%) is subhedral and microperthitic. Feldspars show low to moderate alteration to sericite and clay minerals. Quartz (10–25 vol%) is mainly anhedral and interstitial to other rock-forming minerals, and is also present in the quartz-feldspathic groundmass. It sometimes appears as rounded embayed crystals, indicating resorption by the melt during magma ascent after a temporary resting in the magma chamber and partial crystallization (Vernon, 2018). Clinopyroxene (5–10 vol%) occurs as subhedral to anhedral phenocrysts, showing alteration to chlorite and opaque minerals. Biotite (0–5 vol%) is euhedral to subhedral (1–2 mm) and shows alteration to chlorite. Amphibole (0–5 vol%) occurs as euhedral and almost fresh phenocrysts. Accessory minerals are apatite, titanite and opaque minerals. The porphyry stock shows porphyritic texture with microgranular groundmass to microlitic porphyritic texture.

The dike swarms in the study area were divided into 2 generations based on their cross-cutting relationship, composition, and general trend. The first generation with NW–SE trend has granodioritic composition, very similar to the porphyry stock (except for not having clinopyroxene), while the second generation with mainly NE–SW trend has monzodioritic–microdioritic composition, and differ from the

Table 3Electron probe micro-analysis (EPMA) results of various ore minerals from the skarn, porphyry and epithermal mineralization zones. The element concentrations are in wt%.

Point. No	1/1	1 / 2	1/3	1 / 4	1/5	1/6	1 / 7	1/8	1/9	1 / 10	1 / 11
Mineral	Сср	Сср	Сср	Сср	Сср	Сср	Сср	Сср	Сср	Сср	Сср
Fe	27.1	21.0	20.0	17.9	30.0	33.3	35.2	29.7	30.3	30.0	29.8
Ag	0.01	0	0	0.02	0	0.02	0.02	0.04	0.01	0.01	0.04
Zn	0	0	0	0.01	0	0	0	0.02	0	0	0
Ni	0	0.01	0	0	0.02	0.02	0.01	0	0	0.01	0
Cu	52.5	53.5	53.2	33.9	31.6	32.7	12.8	34.0	34.0	33.9	33.5
S	20.0	26.0	22.0	35.0	30.0	30.0	40.0	34.4	34.3	35.2	34.7
Co	0	0	0	0	0	0	0	0	0	0	0
As Te	0.02	0	0	0.03 0	0.03 0	0	0.03 0.01	0.03 0.06	0.01 0	0.01	0
	0.02	0	0.03	0.03	0.08	0.07	0.01	0.00	0.01	0.01	0.03
Au Si	0.02	0	0.03	2.25	5.06	3.53	3.58	0	0.01	0.01	0.03
Sb	0.02	0.01	0	0.02	0	3.53 0	3.58 0	0	0.01	0	0.02
Ba	0.05	0.01	0.03	0.02	0.16	0.03	0.01	0.02	0.03	0.02	0.02
Total	99.7	100.6	95.2	89.2	96.9	99.6	91.7	98.2	98.6	99.1	98.1
Atomic proportions		100.0	93.2	69.2	90.9	99.0	91.7	90.2	96.0	99.1	90.1
Fe	0.6	0.46	0.44	0.39	0.66	0.74	0.78	0.66	0.67	0.66	0.66
	0.0	0.40	0.44	0.39	0.00	0.74	0.78	0.00	0.67	0.00	0.00
Ag											
Zn	0	0	0	0	0	0	0	0	0	0	0
Ni Cu											
	0.82	0.84	0.83	0.53	0.49	0.51	0.2	0.53	0.53	0.53	0.52
S	0.62	0.81	0.86	1.09	0.93	0.93	1.24	1.07	1.07	1.09	1.08
Co	0	0	0	0	0	0	0	0	0	0	0
As	0	0	0	0	0	0	0	0	0	0	0
Te	0	0	0	0	0	0	0	0	0	0	0
Au c:	0	0	0	0	0	0	0	0	0	0	0
Si	0	0	0	0.08	0.18	0.12	0.12	0	0	0	0
Sb	0	0	0	0	0	0	0	0	0	0	0
Ba	0	0	0	0	0	0	0	0	0	0	0
Porphyry system Point.No	1 / 12	1 / 13		1 / 14	1 / 15	1 / 16	1 / 17		1 / 18	1 / 19	1 / 20
Mineral	Py.	Py.		Py.	Py.	Py.	Py.		Py.	Py.	Py.
Si	0	0		0	0	0.34	0.03	()	0.02	0
S	53.45	52.75		53.30	52.75	52.54	52.88	į	52.59	52.76	52.70
Fe	45.22	45.51		45.83	45.22	45.46	47.76	4	47.42	47.31	47.31
Co	0	0		0	0	0	0	()	0	0
Ni	0	0.43		0	0	0	0.03	(0.02	0	0.02
Cu	1.00	0.70		0.58	0	0.51	0.28	(0.01	0.09	0.01
Zn	0.03	0.11		0.11	0.20	0.10	0	(0.02	0	0.01
As	0	0.08		0.09	0.03	0.72	0.05	(0.05	0.01	0.09
Mo	0.01	0		0.01	0	0	0	()	0	0
Ag	0	0		0	0	0	0	(0.01	0	0
Cd	0	0		0	0	0	0.06	()	0	0
Sb	0	0		0	0	0.20	0.02	()	0	0.02
W	0	0.01		0	0	0.02	0.04	()	0.12	0
Au	0	0		0	0	0	0)	0	0
Hg	0	0.04		0	0.04	0	0.11)	0	0.04
Pb	0.21	0.11		0.28	0.37	0.14	0)	0	0
Bi	0.14	0.24		0.05	0.33	0.17	0.03		0.06	0.01	0.03
Te	0	0.03		0.03	0	0.03	0.08)	0.06	0.10
Ca	0	0		0	0	0	0.01		0.02	0	0
	0	0		0	0	0	0)	0	0
		U				100.26	101.40		100.20	100.40	100.3
Mn				100.35	99.00			-			
Mn Total	100.60	100.05		100.35	99.00	100.20					
Mn Total Atomic proportions Si	100.60			0			0	()	0	
Mn Total Atomic proportions Si	100.60 s 0	100.05 0		0	0	0	0 1.64) 1.64		0
Mn Total Atomic proportions Si S	100.60 s 0 1.70	100.05 0 1.64		0 1.66	0 0	0 0	1.64		1.64	1.64	0 1.64
Mn Total Atomic proportions Si S Fe	100.60 s 0 1.70 0.82	100.05 0 1.64 0.82		0 1.66 0.82	0 0 1.64	0 0 1.63	1.64 0.85	:	1.64).84	1.64 0.84	0 1.64 0.84
Mn Total Atomic proportions Si S Fe Co	100.60 s 0 1.70 0.82	100.05 0 1.64 0.82 0		0 1.66 0.82	0 0 1.64 0.82	0 0 1.63 0.82	1.64 0.85 0	; (1.64).84)	1.64 0.84 0	0 1.64 0.84
Mn Total Atomic proportions Si S Fe Co Ni	100.60 s 0 1.70 0.82 0	100.05 0 1.64 0.82 0		0 1.66 0.82 0	0 0 1.64 0.82	0 0 1.63 0.82	1.64 0.85 0	(1.64 0.84 0	1.64 0.84 0	0 1.64 0.84 0
Mn Total Atomic proportions Si S Fe Co Ni Cu	100.60 s 0 1.70 0.82 0 0 0.01	100.05 0 1.64 0.82 0 0		0 1.66 0.82 0 0	0 0 1.64 0.82 0	0 0 1.63 0.82 0	1.64 0.85 0 0	(1.64 0.84 0 0	1.64 0.84 0 0	0 1.64 0.84 0 0
Mn Total Atomic proportions Si S Fe Co Ni Cu Zn	100.60 s 0 1.70 0.82 0 0 0.01	100.05 0 1.64 0.82 0 0 0		0 1.66 0.82 0 0	0 0 1.64 0.82 0 0	0 0 1.63 0.82 0 0	1.64 0.85 0 0 0	(1.64 0.84 0 0 0	1.64 0.84 0 0 0	0 1.64 0.84 0 0 0
Mn Total Atomic proportions Si S Fe Co Ni Cu Zn As	100.60 s 0 1.70 0.82 0 0 0.01 0 0	100.05 0 1.64 0.82 0 0 0 0		0 1.66 0.82 0 0 0 0	0 0 1.64 0.82 0 0 0	0 0 1.63 0.82 0 0 0	1.64 0.85 0 0 0 0	(1.64 0.84 0 0 0 0 0	1.64 0.84 0 0 0 0	0 1.64 0.84 0 0 0
Mn Total Atomic proportions Si S Fe Co Ni Cu Zn As	100.60 s 0 1.70 0.82 0 0 0.01 0 0 0 0 0	100.05 0 1.64 0.82 0 0 0 0 0		0 1.66 0.82 0 0 0 0 0	0 0 1.64 0.82 0 0 0	0 0 1.63 0.82 0 0 0	1.64 0.85 0 0 0 0 0		1.64 0.84 0 0 0 0 0	1.64 0.84 0 0 0 0 0	0 1.64 0.84 0 0 0 0
Mn Total Atomic proportions Si Fe Co Ni Cu Zn As Mo Ag	100.60 s 0 1.70 0.82 0 0 0.01 0 0	100.05 0 1.64 0.82 0 0 0 0 0		0 1.66 0.82 0 0 0 0 0 0 0	0 0 1.64 0.82 0 0 0 0	0 0 1.63 0.82 0 0 0 0	1.64 0.85 0 0 0 0 0		1.64 0.84 0 0 0 0 0 0 0	1.64 0.84 0 0 0 0 0 0	0 1.64 0.84 0 0 0 0 0 0
Mn Total Atomic proportions Si S Fe Co Ni Cu Zn As Mo Ag Cd	100.60 s s 0 1.70 0.82 0 0 0.01 0 0 0 0 0 0 0 0 0 0 0 0 0 0 0	100.05 0 1.64 0.82 0 0 0 0 0 0		0 1.66 0.82 0 0 0 0 0 0	0 0 1.64 0.82 0 0 0 0 0	0 0 1.63 0.82 0 0 0 0 0	1.64 0.85 0 0 0 0 0 0 0		1.64 0.84 0 0 0 0 0 0 0	1.64 0.84 0 0 0 0 0 0 0	0 1.64 0.84 0 0 0 0 0 0 0
Mn Total Atomic proportions Si S Fe Co Ni Cu Zn As Mo Ag Cd	100.60 s 0 1.70 0.82 0 0 0.01 0 0 0 0 0 0 0 0 0 0 0 0 0 0 0	100.05 0 1.64 0.82 0 0 0 0 0 0 0		0 1.66 0.82 0 0 0 0 0 0 0 0	0 0 1.64 0.82 0 0 0 0 0 0	0 0 1.63 0.82 0 0 0 0 0 0	1.64 0.85 0 0 0 0 0 0 0 0		1.64).84)))))))))))	1.64 0.84 0 0 0 0 0 0 0 0 0	0 1.64 0.84 0 0 0 0 0 0 0 0
Mn Total Atomic proportions Si S Fe Co Ni Cu Zn As Mo Ag Cd Sb	100.60 s 0 1.70 0.82 0 0 0.01 0 0 0 0 0 0 0 0 0 0 0 0 0 0 0	100.05 0 1.64 0.82 0 0 0 0 0 0 0		0 1.66 0.82 0 0 0 0 0 0 0 0 0	0 0 1.64 0.82 0 0 0 0 0 0 0	0 0 1.63 0.82 0 0 0 0 0 0 0	1.64 0.85 0 0 0 0 0 0 0 0		1.64).84))))))))))))	1.64 0.84 0 0 0 0 0 0 0 0 0	0 1.64 0.84 0 0 0 0 0 0 0 0
Mn Total Atomic proportions Si S Fe Co Ni Cu Zn As Mo Ag Cd Sb W Au	100.60 s 0 1.70 0.82 0 0.01 0 0 0 0 0 0 0	100.05 0 1.64 0.82 0 0 0 0 0 0 0 0		0 1.66 0.82 0 0 0 0 0 0 0 0 0 0	0 0 1.64 0.82 0 0 0 0 0 0 0 0	0 0 1.63 0.82 0 0 0 0 0 0 0 0	1.64 0.85 0 0 0 0 0 0 0 0 0		1.64).84))))))))))))	1.64 0.84 0 0 0 0 0 0 0 0 0 0	0 1.64 0.84 0 0 0 0 0 0 0 0
Mn Total Atomic proportions Si S Fe Co Ni Cu Zn As Mo Ag Cd Sb	100.60 s 0 1.70 0.82 0 0 0.01 0 0 0 0 0 0 0 0 0 0 0 0 0 0 0	100.05 0 1.64 0.82 0 0 0 0 0 0 0		0 1.66 0.82 0 0 0 0 0 0 0 0 0	0 0 1.64 0.82 0 0 0 0 0 0 0	0 0 1.63 0.82 0 0 0 0 0 0 0	1.64 0.85 0 0 0 0 0 0 0 0		1.64).84))))))))))))	1.64 0.84 0 0 0 0 0 0 0 0 0	0 1.64 0.84 0 0 0 0 0 0 0 0

(continued on next page)

Mn Total

98.79

Table 3 (continued) Porphyry system

Porphyry system Point.No	1 / 12	1 / 13	1/	14	1 / 15	1 / 16	1/	17	1 / 18	1 / 19	1 / 20
Те	0	0	0		0	0	0		0	0	0
Ca	0	0	0		0	0	0		0	0	0
Mn	0	0	0		0	0	0		0	0	0
Porphyry system Point. No	2/1	2/2	2/3	2 / 4	2/5	2/6	2/7	2/8	2/9	2 / 10	2/1
Mineral	Ttr.	Ttr.	Ttr.	Ttr.	Ttr.	Ttr.	Ttr.	Ttr.	Ttr.	Ttr.	Ttr.
i	0.08	0.5	0	0	0	0	0.58	0.18	0.19	0	0.77
1	23.0	22.0	24.9	25.5	24.8	24.6	24.6	27.0	22.0	24.9	24.9
e e	0.07	0.09	0.27	0.32	0.21	0.26	0	3.01	0.06	0.27	0.27
Со	0	0	0	0	0	0	0	0	0	0	0
Ii	0	0	0	0	0	0	0	0.02	0	0	0
Cu	20.0	21.7	37.8	38.5	37.3	37.2	10.8	40.6	26.2	37.4	37.9
Zn	0.13	0.16	5.6	5.57	5.21	5.19	0	3.78	0	5.33	5.38
As	0.7	0.9	4.6	7.5	3.0	3.8	8.0	18.9	12.8	3.4	5.7
Ло	0.2	0.9	0.0	0	0	0	0.1	0.2	0.3	0	0
Ag	0	0	0.8	0.8	1.31	1.49	0.05	0.2	0.22	1.59	1.11
Cd .	0.09	0.04	0.07	0.01	0.05	0.08	0	0.03	0.06	0.11	0.05
Sb	1.6	2.2	23.6	19.9	26.9	25.3	23.0	3.8	7.2	25.7	22.7
V	0.02	0	0.11	0	0	0	0	0	0.08	0	0
Au	0.04	0.04	0	0.32	0.25	0.02	0.08	0	0.01	0.03	0.64
łg	0	0	0	0	0	0.17	0	0	0	0	0.02
rb	51.9	51.0	0.0	0.0	0.0	0.0	26.2	2.0	31.0	0.0	0.0
Bi	0	0	0	0	0	0	0	0.38	0	0	0
Ге	0.33	0.51	0.1	0	0.02	0.17	3.51	0.4	0.08	0.11	0.03
Ca	0.38	0.47	0	0	0	0.17	2.12	0	0.63	0	0.00
Иn	0	0	0.02	0.01	0.01	0	0	0	0	0.01	0.04
Γotal	98.4	100.4	97.8	98.3	99.0	98.3	99.0	100.5	100.8	98.9	99.5
Atomic proportion											
Si	0	0	0	0	0	0	0	0	0	0	0
3	0.71	0.68	0.77	0.79	0.77	0.76	0.76	0.84	0.68	0.77	0.77
Fe .	0	0	0	0.75	0	0.70	0	0.03	0.00	0	0.77
Со	0	0	0	0	0	0	0	0.03	0	0	0
Ni	0	0	0	0	0	0	0	0	0	0	0
Cu	0.31	0.34	0.59	0.6	0.58	0.58	0.16	0.63	0.41	0.58	0.59
Zn	0.51	0.54	0.08	0.08	0.07	0.07	0.10	0.05	0.41	0.08	0.08
	0	0.01	0.06	0.09	0.07	0.05	0.1	0.05	0.1	0.03	0.03
As	0	0.01	0.06		0.03	0.05			0.1	0.04	0.07
Mo	0	0	0	0			0 0	0	0	0.01	
Ag					0.01	0.01		0			0.01
Cd	0	0	0	0	0	0	0		0	0	0
Sb	0.01	0.01	0.19	0.16	0.22	0.2	0.18	0.03	0.05	0.21	0.18
W	0	0	0	0	0	0	0	0	0	0	0
Au	0	0	0	0	0	0	0	0	0	0	0
Hg	0	0	0	0	0	0	0	0	0	0	0
Pb	0.25	0.24	0	0	0	0	0.12	0	0.1	0	0
Bi	0	0	0	0	0	0	0	0	0	0	0
Ге	0	0	0	0	0	0	0.02	0	0	0	0
Ca	0	0	0	0	0	0	0.02	0	0	0	0
Mn	0	0	0	0	0	0	0	0	0	0	0
	Skarn	0.40	0.74	0.41	-	Epithermal sy	<u>'</u>	0.46	0 / 1	0.40	
Point. No	3 / 1	3 / 2	3 / 4	3 / 5	•	8 / 4	8 / 5	8/6	8 / 1	8 / 2	8 /
Mineral	Gn.	Gn.	Gn.	Gn.		Py.	Py.	Py.	Gold	Gold	Gol
Si	0.09	0.1	0.03	0.18		0.05	0.03	0.03	0.13	0.09	0.0
3	17.54	12.58	14.33	16.0		52.37	52.76	53.23	0.03	0.04	0.0
e e	2.79	4.03	1.72	2.49		47.6	47.52	46.2	0.06	0.03	0
Со	0	0	0.02	0		0	0	0	0.03	0	0.0
Ni	0	0.4	0.02	0		0	0.01	0	0	0.01	0
Cu	1.55	1.07	0	0.04		0	0	0.08	0.08	0	0.0
Zn	0	0.09	0	0.03		0.01	0.05	0	0	0	0
As	0	0.07	0	0		0.03	0.03	0	0	0	0
Ло	0.12	0.09	0	0		0	0	0	0	0	0
Λg	0	0	0	0		0	0.02	0	2.54	0.15	3.9
Cd .	0	0.11	0	0.11		0.03	0.05	0.01	0	0	0
Sb	0	0	0.02	0.07		0	0	0	0.3	0	0
N	0	0	0.12	0.19		0.01	0.07	0	0	0	0
Au	0	0	0	0.17		0.01	0.07	0.05	94.1	96.5	93.
-Ig	0	0.07	0.05	0.06		0.21	0	0.03	0	0	0
rg Pb	75.71	78.17	81.86	79.1		0.21	0	0.05	0	0	0
o Bi	75.71 0.94						0.16			0.04	0.0
		0.62	0.21	0.21		0.09		0	0.03		
Ce	0.05	0.03	0.13	0.14		0	0.03	0.04	0.02	0	0
Ca	0	0	0	0		0.01	0.02	0.07	0	0	0
/In	0	0	0	0		0.01	0	0	0	0	0
Total	98.79	97.43	98.51	98.7	h	100.4	100.8	99.76	97.3	96.8	97.6

(continued on next page)

97.6

96.8

97.3

99.76

100.4

100.8

0 98.51

97.43

98.76

Table 3 (continued)

	Skarn				Epitherm	Epithermal system						
Point. No	3 / 1	3 / 2	3 / 4	3 / 5	8 / 4	8 / 5	8 / 6	8 / 1	8 / 2	8 /		
Atomic proportion	ons											
Si	0	0	0	0	0	0	0	0.01	0	0		
3	0.82	0.4	0.32	0.32	1.63	1.64	1.56	0	0	0		
Fe	0.04	0.06	0.44	0.5	0.85	0.85	0.82	0	0	0		
Со	0	0	0	0	0	0	0	0	0	0		
Ni	0	0	0	0	0	0	0	0	0	0		
Cu	0.09	0.08	0	0	0	0	0.04	0	0	0		
Zn	0	0	0	0	0	0	0	0	0	0		
AS	0	0	0	0	0	0	0	0	0	0		
Мo	0	0	0	0	0	0	0	0	0	0		
Ag	0	0	0	0	0	0	0	0.02	0	0.		
Cd	0	0	0	0	0	0	0	0	0	0		
Sb	0	0	0	0	0	0	0	0	0	0		
N	0	0	0	0	0	0	0	0	0	0		
Au	0	0	0	0	0	0	0	0.47	0.48	0.		
-Ig	0	0	0	0	0	0	0	0	0	0		
ъ	0.33	0.3	0.39	0.38	0	0	0	0	0	0		
i	0	0	0	0	0	0	0	0	0	0		
`e	0	0	0	0	0	0	0	0	0	0		
Ca	0	0	0	0	0	0	0	0	0	0		
ſn	0	0	0	0	0	0	0	0	0	0		
	Epitl	hermal system										
oint No	5 / 1	•	5/2 5/3		5/4		5/5	5/6		5 /		
/lineral	Stb.		Stb.	Stb.		Stb.	Stb.	Stl		St		
i	0.8		0	0		0	0	0.0		0		
-	24.3		21.64	16.28		22.98	20.04	18.		19		
'e	0.02		0	0		0.01	0	0.0		0		
Co	0.02		0	0		0	0	0.0		0		
Ni	0		0	0.01		0.01	0.01	0.0		0.0		
Cu	0.11		0	0.03		0.05	0.12	0.7		0.9		
in		0		0.03		0.02	0.01		0.03			
As	2.64		0.05 2.57	4.2		3.32	3.29	2.5		0 4.3		
	0		0	0		0.02	0.09	0	•	0		
Mo N ~	0		0	0.02		0.02	0.09	0		0.0		
Ag Cd	0		0	0.02		0	0	0.0	11	0.0		
	61.2	n	65.09									
b	0	2		70.05		67.16	68.08	63.	.05	62		
V			0	0.03		0	0	0		0		
u •	9.98		10.43	9.86		6.07	8.09	12		10		
lg	0.05		0.03	0.06		0.17	0.01	4.0	19	3.2		
b	0		0	0		0.03	0	0		0		
i	0		0	0		0	0	0		0		
`e	0.01		0	0		0.05	0	0.2	1	0		
a	0		0	0		0	0	0		0		
In .	0.02		0.02	0		0	0	0	_	0		
otal	99.1° Atom	/ nic proportions	99.83	100.6		99.89	99.74	10	I	99		
i	0.02		0	0		0	0	0		0		
	0.75	8	0.675	0.508		0.717	0.625	0.5	571	0.		
e	0		0	0		0	0	0		0		
0	0		0	0		0	0	0		0		
i	0		0	0		0	0	0		0		
u	0		0	0		0	0	0.0)1	0.		
n	0		0	0		0	0	0		0		
s	0.03		0.03	0.05		0.04	0.04	0.0	3	0.		
ſо	0		0	0		0	0	0		0		
g	0		0	0		0	0	0		0		
d	0		0	0		0	0	0		0		
b	0.50	3	0.535	0.575		0.552	0.559	0.5	18	0.		
I	0.30.	•	0.333	0.373		0.332	0.339	0.3	.10	0.		
				0.05		0.03		0.0	16			
u	0.05		0.05				0.04			0.		
g	0		0	0		0	0	0.0	12	0.		
ь	0		0	0		0	0	0		0		
i	0		0	0		0	0	0		0		

porphyry stock and the first generation dikes by having higher amphibole content, which occasionally reaches up to 25 vol%, lower quartz content and the lack of clinopyroxene. The second generation dikes are comprised of plagioclase (30–60 vol%, both as phenocrysts of 0.5–2 mm size, and as microlites), amphibole (up to 25 vol%), biotite (0–5 vol%),

Bi

Те

Ca

and fine-grained quartz (<10 vol%) (Fig. 3e). Accessory minerals are titanite, apatite and opaque minerals. Both dike series display porphyritic to microlitic porphyritic textures.

The sills consist of plagioclase (20–35 vol%), amphibole (5–15 vol%), quartz (0–5 vol%) and opaque (up to 4 vol%; including euhedral

pyrite) minerals (Fig. 3f). The modal composition in central parts of the thick sills is monzodioritic, while in marginal parts or in thinner ones, they are mainly andesitic.

4.2. Metamorphism

Based on field observations, emplacement of the high-temperature porphyry stock within the upper Cretaceous—Paleocene flysch-type host rocks has produced a narrow contact metamorphic zone along the contact, as well as skarn patches and metasomatic alteration. Within the contact metamorphic zone, the flysch-type rocks have consequently been transformed into marble, hornfels, calc-silicate hornfels and metapelite. Fine-grained garnet and pyroxene have been formed within the marble and hornfels, respectively.

Hornfels rocks were resulted from non-calcareous rocks, including shale and siltstone and their primary bedding is preserved to some extent. Moreover, they display bright and dark colored banding. Calc-silicate hornfels rocks were originated from calcareous marls, which have brighter color compared to hornfels rocks. However, their primary bedding was obliterated. In general, marble and hornfels rocks do not contain any mineralization, except fine and disseminated anhedral pyrite within the hornfels rocks.

4.3. Metasomatic alteration

Metasomatic alteration caused by evolving fluids derived from porphyry stock is characterized by the formation of endo- and exoskarn zones in and around the intrusive body, respectively. An endoskarn zone was formed within the marginal part of the intrusive body, in contact with the flysch-type country rocks. This zone is almost restricted to a narrow strip along the contact, ranging in thickness from 0.2 to 1 m. Petrographically, this zone includes a metasomatic alteration assemblage consisted of epidote, tremolite–actinolite, chlorite, and calcite, besides the primary igneous minerals (Fig. 4a). The primary texture of the intrusive rock is generally preserved in this zone, though in some

places, the entire rock is replaced by massive moss green epidote, causing the full obliteration of the original texture. Oxide (magnetite) and sulfide (pyrite, chalcopyrite and rarely bornite) ore minerals are also locally present within the endoskarn zone.

The exoskarn zone has a variable thickness, and shows massive and banded structures. Based on petrographic observations, the massive skarn mainly appears as epidote skarn, with lesser garnet crystals (Fig. 4b). However, this zone contains coarser crystals of brown to yellow garnet, the size of which increases towards the intrusive body. Its main outcrops are found at Sildirimdara, Kaghdara and rarely Boiokwari areas. EPMA analyses on garnets indicate that they belong to the andradite species. Wollastonite is also present in this zone, mainly accompanied by calcite. Oxide and sulfide mineralization includes magnetite, pyrite, chalcopyrite, bornite and galena–sphalerite, occurring as veinlets, disseminations and also locally massive patches.

The banded exoskarn zone (ranging in thickness from 5 to 40 m) is distal relative to the massive zone and terminates to hornfels and unmetamorphosed flysch-type rocks. However, the boundary between them is neither sharp nor clear. It is mainly cropped out at Boiokwari and to lesser extent at Nowrozkala. It extends up to 300–400 m from the intrusive body and shows alternations of fine-grained olive-yellow and gray colored calc-silicate bands (each band 5–30 cm thick), corresponding to calcareous sandstone and silty shale within the protolith (Fig. 4a). Compared to endoskarn and massive exoskarn zones, this zone does not contain significant ore minerals, except some scarce quartz veinlets with altered pyrites.

Finally, during the retrograde stage and following the alteration of anhydrous calc-silicates (garnet, pyroxene), hydrous calc-silicates such as tremolite-actinolite and epidote, along with quartz, chlorite, clay minerals and calcite have been formed in the skarn zones.

4.4. Hydrothermal alterations of porphyry system

The Oligo–Miocene porphyry stock in the Astarghan area was affected by hydrothermal fluids and suffered several types of alterations.

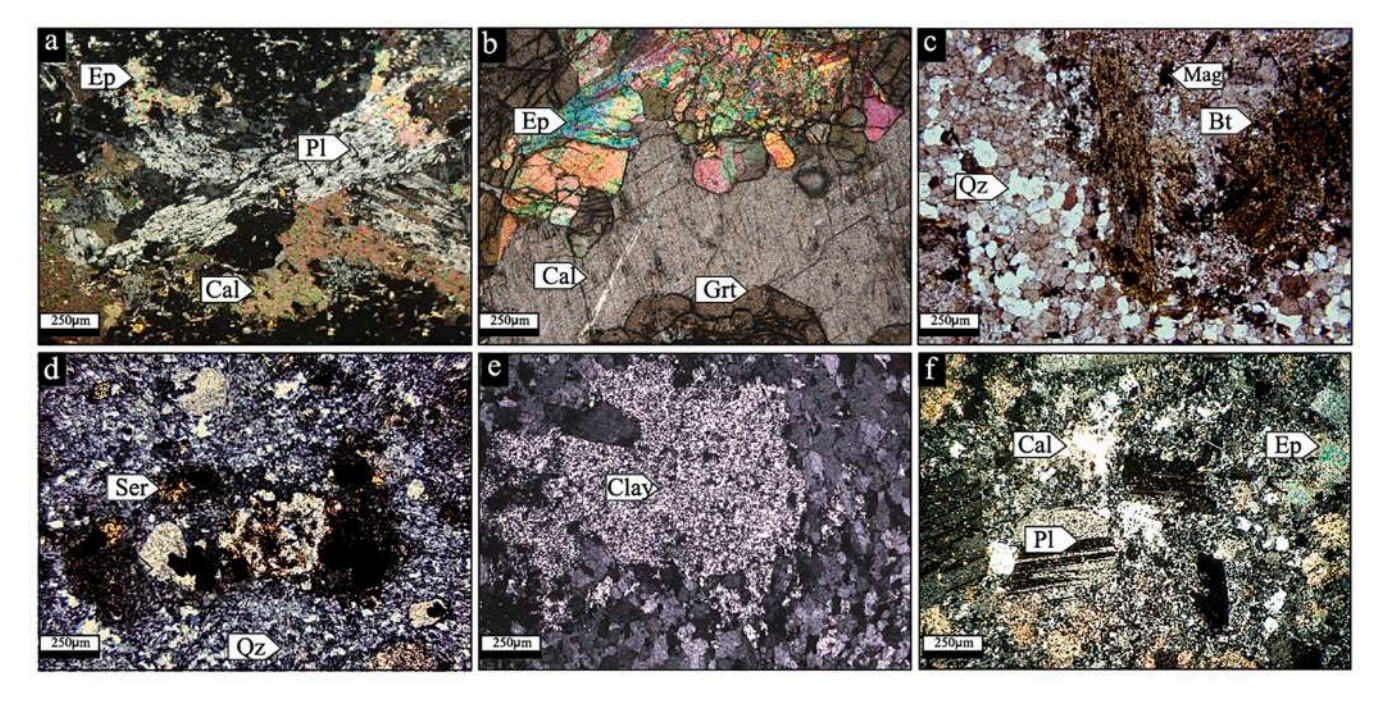


Fig. 4. Photomicrographs of various alteration zones. (a) A plagioclase being altered to epidote and calcite in the endoskarn zone (XPL). (b) Formation of garnet, calcite and epidote in the exoskarn zone (XPL). (c) Alteration of ferro-magnesian minerals to secondary biotite flakes and magnetite in the potassic zone (XPL). (d) Sericitization of feldspars and formation of opaque minerals (mainly pyrite) in the phyllic zone (XPL). (e) Complete alteration of feldspars to clay minerals in the argillic zone (XPL). (f) Alteration of plagioclase and ferro-magnesian minerals to calcite and epidote in the propylitic zone (XPL). Mineral abbreviations are from Whitney and Evans (2010).

The main hydrothermal alterations in the area comprise porphyry-type potassic, phyllic, argillic, and propylitic zones within the porphyry stock. However, their typical zonation pattern is obliterated due to severe faulting and therefore, outcrops of various alteration zones show irregular distribution.

4.4.1. Potassic alteration zone

This alteration zone is best observed at Kaghdara and Boiokwari areas (Zone B; see Fig. 2). It occurs within the inner part of the porphyry stock. The patches of this alteration are also observed as lenses surrounded by phyllic alteration assemblage. The main minerals in this zone are secondary biotite and orthoclase, accompanied by lesser magnetite (Fig. 4c). Additionally, various generations of quartz–sulfide veinlets were developed within this zone. Sulfides are mainly pyrite, chalcopyrite, bornite, and rarely molybdenite. Petrographic examination showed that magmatic biotite and amphibole were replaced by secondary biotite flakes, which were in turn altered to chlorite (Fig. 4c).

4.4.2. Phyllic alteration zone

This alteration is best observed at Sildirimdara area (Fig. 2) and in general, has a limited spatial distribution in the Astarghan area. It is mainly developed in wall rocks of the quartz–tetrahedrite veins/veinlets, where it grades outwardly to argillic zone. The alteration assemblage consists of sericite, quartz and pyrite. Fine-grained sericite is the result of the alteration of feldspars (especially plagioclase; Fig. 4d). Plagioclase was altered to sericite and sometimes to clay minerals. In some parts such as the Boiokwari area, both sericite and secondary biotite are present, which can be interpreted as a zone of transitional potassic–phyllic alteration, formed by partial overprinting of the phyllic alteration on the early-formed potassic assemblage.

4.4.3. Argillic alteration zone

The porphyry-related argillic alteration zone was mainly developed at Nowrozkala, within and around the brecciated zones in the porphyry stock (caused by tectonic activities and fault movements) and shows spatial relationship with the phyllic alteration zone (Fig. 2). Hand specimens from this zone have grayish white color. XRD analysis on the samples taken from this zone shows the presence of kaolinite, illite, dickite and quartz, along with lesser sericite. All the feldspars were altered to clay minerals (Fig. 4e), inasmuch as only their outline is recognizable under microscope. Meanwhile, clay minerals have also been formed within the groundmass of the intrusive body in this zone, along with minor sericite and quartz.

Some superficial samples of argillic alteration zone contain jarosite, natrojarosite and iron oxides/hydroxides (according to XRD data), which can be attributed to supergene alteration superimposed on the phyllic assemblage. The existence of supergene iron oxides and hydroxides within this zone impart red, yellow and orange colors to the surficial outcrops.

4.4.4. Propylitic alteration zone

The propylitic assemblage is mainly found at the peripheral parts of the porphyry stock. This alteration is also pronounced within the dikes. The alteration assemblage in this zone includes epidote, calcite, tremolite and chlorite (Fig. 4f). Plagioclase phenocrysts were partially replaced by epidote or sericite. Almost all ferromagnesian minerals (hornblende and biotite) are altered to chlorite, calcite, epidote and magnetite. Pyrite is the only sulfide present in this zone.

4.5. Hydrothermal alteration related to the epithermal veins/veinlets

The epithermal Au–Sb vein-type mineralization is mainly found in Nowrozkala, where the prevalent alterations around the veins/veinlets within the host wall rocks (the porphyry stock) occurred as chiefly silicic and argillic halos, spreading as irregular dispersed patches in a vast area

(Fig. 2). Feldspars in the argillic selvage were severely altered to clay minerals. Alunite has also been identified within some samples by XRD analysis in the argillic envelope.

4.6. Mineralization

The precious and base metal mineralization in the Astarghan area occurred in three main zones, (1) copper–lead–zinc skarn patches (Zone A; Fig. 2), (2) porphyry-type copper–(gold) stockwork veins/veinlets, mainly associated with the potassic zone, and quartz–tetrahedrite veins/veinlets related to the phyllic alteration (Zone B; Fig. 2), and (3) gold–stibnite epithermal mineralization associated with the argillic alteration zone (Zone C; Fig. 2).

4.6.1. Skarn-type mineralization

The main outcrops of the skarn patches are observed in the Kaghdara area, southeast of the porphyry stock, within the upper Cretaceous–Paleocene flysch-type rocks. They display two distinct textures: (1) massive and (2) banded. The banded skarn (Fig. 5a), comprised of green and gray bands, crops out in the Kaghdara and Boiokwari areas. Mineralization within the banded skarn occurred as quartz–sulfide veins/veinlets (<20 cm thick, 15–20 m long, trending northwest and northeast) containing pyrite and scarce chalcopyrite, along with supergene minerals of goethite and limonite. Au grade in some of these veins/veinlets reaches up to 2 ppm. Although the banded skarn has no appreciable economic interest, the quartz–sulfide veinlets, together with the related supergene products, are locally mined from these rocks (Fig. 5a).

Mineralization within the massive skarn includes pyrite, chalcopyrite, bornite, sphalerite and galena accompanied by magnetite and hematite. Sulfides occur as either interstitially disseminated or fracturefilling, as well as replacing the pre-existing minerals, such as magnetite. Chalcopyrite is the main ore mineral and mostly replaces pyrite, locally shows intergrowth with sphalerite and galena, and is in turn replaced by supergene minerals such as covellite, hematite, goethite, malachite and azurite (Fig. 5b). Both pyrite and chalcopyrite show intimate relationship with garnet and epidote, inasmuch as chalcopyrite locally fills the fractures within the garnet crystals, indicating its laterstage occurrence. Magnetite is mainly euhedral, occurring as veinlets or replacing the primary skarn minerals, such as garnet (the latter locally appears as islands surrounded by magnetite) and in turn, shows martitization and replacement by sulfides. Hematite is both hypogene and supergene; the former is found around the garnets, and the latter is formed by supergene alteration of sulfide minerals.

The textural relationship revealed that Cu mineralization in the skarn zones was preceded by Fe and followed by Pb–Zn mineralization. The maximum grade of Cu, Au and Ag in the massive skarn zone are >1 wt%, 0.7 ppm, and 23 ppm, respectively. According to Einaudi et al. (1981), most of the skarn deposits contain some quantity of gold, while it is closely associated with almost all porphyry copper deposits. This was also the case in the Astarghan deposit.

4.6.2. Porphyry-type mineralization

Stockwork veinlets in the Kaghdara and Boiokwari areas: The anastomosing quartz veinlets known as stockworks occurred within the granodiorite to quartz-monzonite porphyry stock at Kaghdara, where the potassic alteration is dominant (Fig. 5c). The stockwork zone is 100-150 m wide and over 200 m long, trending north and dipping 10° eastward. The quartz veinlets vary in thickness from 0.5 cm to 2 cm.

The major sulfide minerals in this zone are pyrite, chalcopyrite, bornite and rarely molybdenite, which also occur as disseminated grains within the groundmass of porphyry stock. Chalcopyrite shows intergrowth with pyrite and also replaces it marginally. Due to the occurrence of later-stage supergene sulfide enrichment, the early hypogene sulfides were replaced by supergene chalcocite and covellite (Fig. 5d). In samples taken from surficial outcrops, alteration of Cu-sulfides to

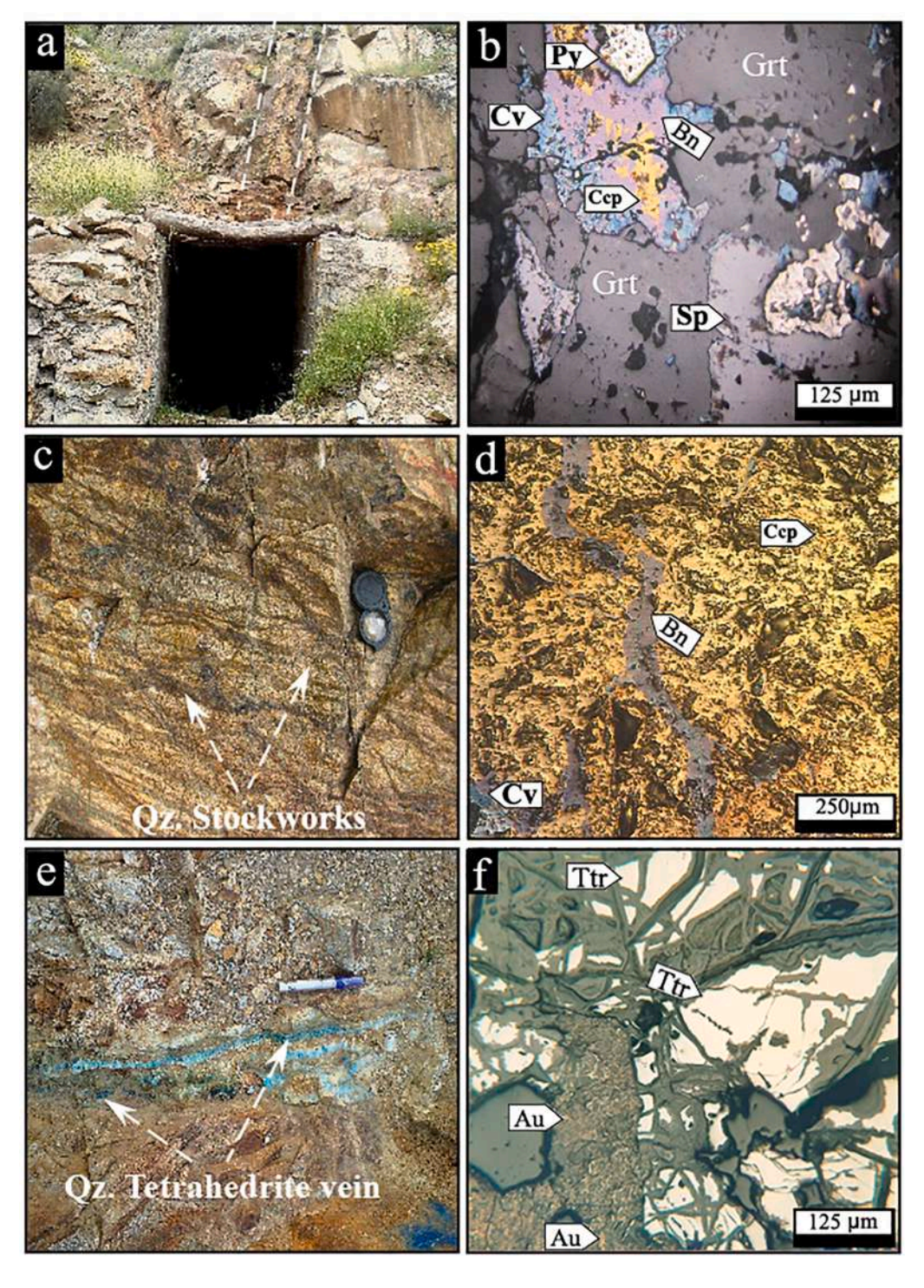


Fig. 5. Field photographs and photomicrographs of various ores from the skarn and porphyry systems. (a) Quartz-iron oxide (most likely altered sulfide) vein within the banded skarn. (b) Replacement of chalcopyrite by bornite and covellite, accompanied by pyrite and sphalerite in massive skarn. (c) Anastomosing veinlets (stockwork) within the potassic alteration zone at Kaghdara. (d) Chalcopyrite replaced by bornite in the porphyry-related potassic zone. (e) Quartz-tetrahedrite veins within the phyllic alteration zone at Sildirimdara. (f) Native gold inclusions within tetrahedrite and its alteration products in the phyllic alteration zone at Sildirimdara. Mineral abbreviations are from Whitney and Evans (2010).

malachite is quite evident. Geochemical analyses show considerable Cu and Au contents of $0.43~\rm wt\%$ and $0.5~\rm ppm$ within these veinlets, respectively.

The Boiokwari stockwork zone is also hosted by the porphyry stock, and located in the northeastern part of the area (at elevation of $\sim 1900\,$ m above the sea level; relatively higher compared to the Kaghdara). The prevalent alteration here is mainly potassic, superimposed by later phyllic assemblage (transitional potassic–phyllic). There are many similarities between the Kaghdara and Boiokwari stockworks in terms of the host rocks and mineralization style. However, the secondary biotite flakes which are common in the Kaghdara stockwork zone are relatively

scarce in Boiokwari, whereas the sericite content is higher in Boiokwari zone. $\,$

Quartz-tetrahedrite veins in the Sildirimdara area: Mineralization at Sildirimdara occurred as quartz-tetrahedrite veinlets within the phyllic alteration zone (Fig. 5e), some of which are altered by supergene processes and contain antimony oxides. The quartz veinlets (3–5 cm thick) have an overall E–W trending and 30–50° dip towards south and contain tetrahedrite (15–25 vol%). They have green and blue appearance on surficial outcrops, resulted from supergene alteration of tetrahedrite to secondary copper minerals such as malachite, azurite and chrysocolla. Quartz crystals within these veinlets display open-space filling, comb,

colloform and massive textures. The most prominent feature of these veinlets is the presence of native gold (5–25 μm in size), which occurs as dispersed fine inclusions within tetrahedrite (Fig. 5f). Moreover, these veinlets have higher Au contents up to 4 ppm.

4.6.3. Epithermal Au-Sb mineralization at Nowrozkala area

The Nowrozkala mineralization zone lies at higher elevation (over 2500 m above the sea level) at the apical part of the porphyry stock. Mineralization in this zone occurred as NE–SW trending quartz–pyrite–stibnite–native gold veins (20–30 cm thick) extending up to 50 m, which are hosted by argillic alteration halo. In addition, there are several quartz–iron oxide veins along the fault zones, fractures and joints, which indicate the remnants of primary pyrite and/or chalcopyrite in these veins. In general, the hypogene metallic minerals in these veins are pyrite, stibnite and native gold, along with supergene assemblage consisted of antimony oxides [valentinite: Sb_2O_3 ; stibiconite $Sb_3O_6(OH)$], hematite, goethite, lepidocrocite, malachite and azurite. Minerals such as cinnabar and realgar are also present in these veins, showing intimate association with antimony oxides and native gold.

Stibnite is present as fine to coarse-grained radial crystals (<5 cm). It is replaced marginally, as well as along the fractures by antimony oxides (valentinite, stibiconite) in some parts. Paragenetically, stibnite is the youngest sulfide and represents the low-temperature epithermal mineralization in this zone. The antimony oxides occur as yellow to green radial aggregates (Fig. 6a). The gangue (mainly quartz) and sulfides display typical comb, honeycomb, crustiform, colloform, cockade, vuggy, drusy, and stockwork textures which are commonly present in epithermal veins/veinlets (Hedenquist et al., 1998) (Fig. 6b).

Pyrite in this zone occurs as disseminated grains within the intrusive body, as well as in association with quartz veins within the host argillic alteration zone. In the surficial outcrops, pyrite is completely oxidized to hematite, goethite and lepidocrocite, producing a honeycomb texture.

Microscopic examinations along with backscattered electron (BSE) images show that native gold occurs in several forms and in several associations: it is interstitially present within the quartz veins of the epithermal mineralization as separate particles (1–3 mm in size;

Fig. 6c–f), in the form of inclusions within or adjacent to stibnites and antimony oxides ($100-150 \mu m$; Fig. 6g), within the euhedral–polyhedral pyrites ($10-50 \mu m$; Fig. 6h), as well as their supergene alteration products, including goethite, hematite and lepidocrocite. Hence, these minerals can be considered as the main hosts for the native gold in these veins and seem to be cogenetic with them. Native gold particles show dendritic, lumpy, rounded, elongate and flaky shapes in cavities lined with iron and antimony-oxides (Fig. 6d–f).

The Au content of antimony oxides is up to 5 ppm, while the overall Au grade within the veins is about 3 ppm. To summarize, the paragenetic sequence of ore minerals in the discussed three major mineralization zones is shown in Fig. 7.

4.7. Fluid inclusion studies

Fluid inclusion studies in the Astarghan deposit were carried out on garnets from the skarn zone, quartz veinlets from the potassic alteration zone at Kaghdara and phyllic zone at Sildirimdara, which represent the porphyry mineralization, as well as the epithermal veins/veinlets at Nowrozkala. Quartz veinlets within the skarn zone contained very fine fluid inclusions ($<4\mu m$), which were not favorable for petrographic examinations and/or microthermometry. On the other hand, fluid inclusions within garnet crystals were rare and very high temperature (2-phase L–V), which were not homogenized even at 600 °C and therefore, fluid inclusion measurements were not performed on skarn-type mineralization.

4.7.1. Petrography of fluid inclusions in porphyry stockwork veinlets at Kaghdara

Samples collected from quartz veinlets in the potassic alteration zone at Kaghdara displayed stockwork texture (0.5–2 cm thick) and contained pyrite and chalcopyrite. Their grayish to dark color was due to the presence of sulfide minerals and mono-phase vapor fluid inclusions. Several generations of these veinlets cross-cut each other, suggesting multiple fracturing and sealing episodes. Quartz grains within these veinlets are fluid inclusion rich, ranging in size from 5 to 30 μm and

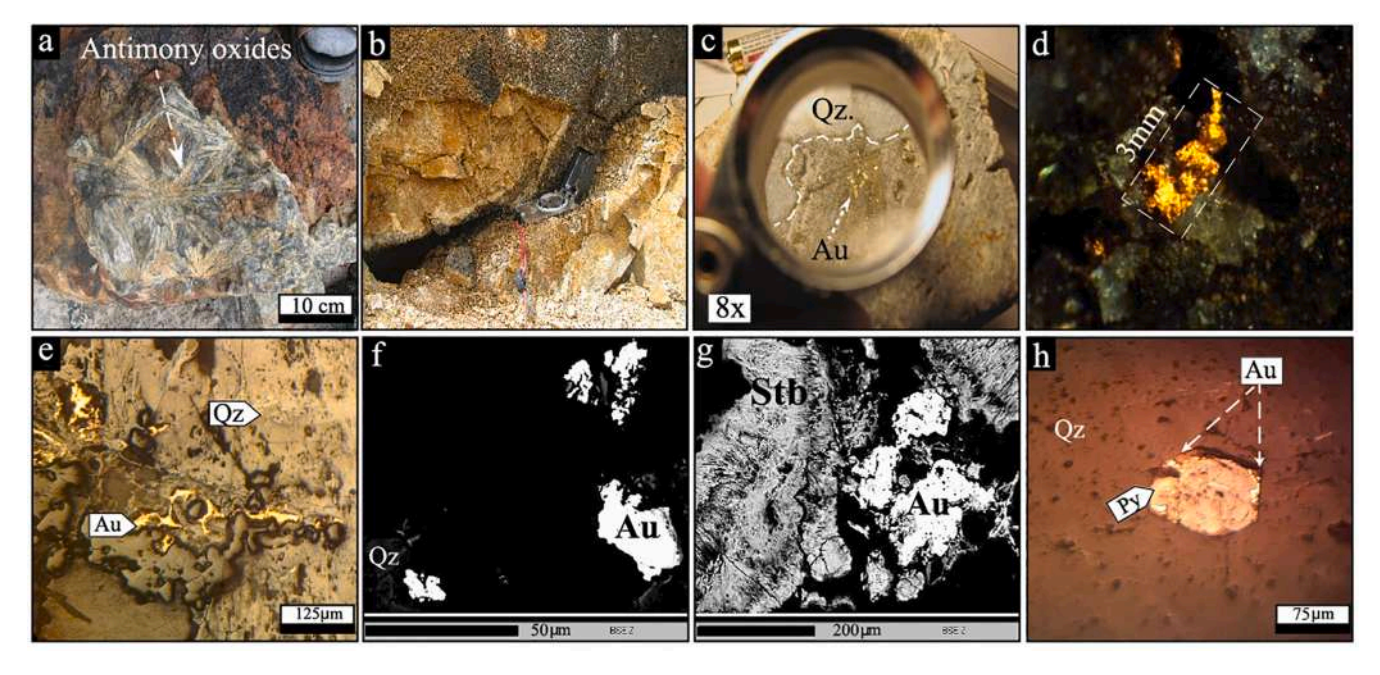


Fig. 6. Field photos and photomicrographs of various ore samples from the epithermal mineralization zone at Nowrozkala. (a) Yellow to gray antimony oxides showing radial aggregate on the surface of quartz-stibnite-native gold veins. (b) Drusy texture within the epithermal veins. (c) Native gold particles (shown by a hand lens) within quartz vein. The lens diameter is 25 mm. (d) Native gold grains within a quartz vein. (e) Dendritic gold within quartz vein. (f) BSE microphotograph of native gold associated with stibnites and antimony oxides. (h) Gold inclusions around a euhedral pyrite within a quartz vein. Mineral abbreviations are from Whitney and Evans (2010).

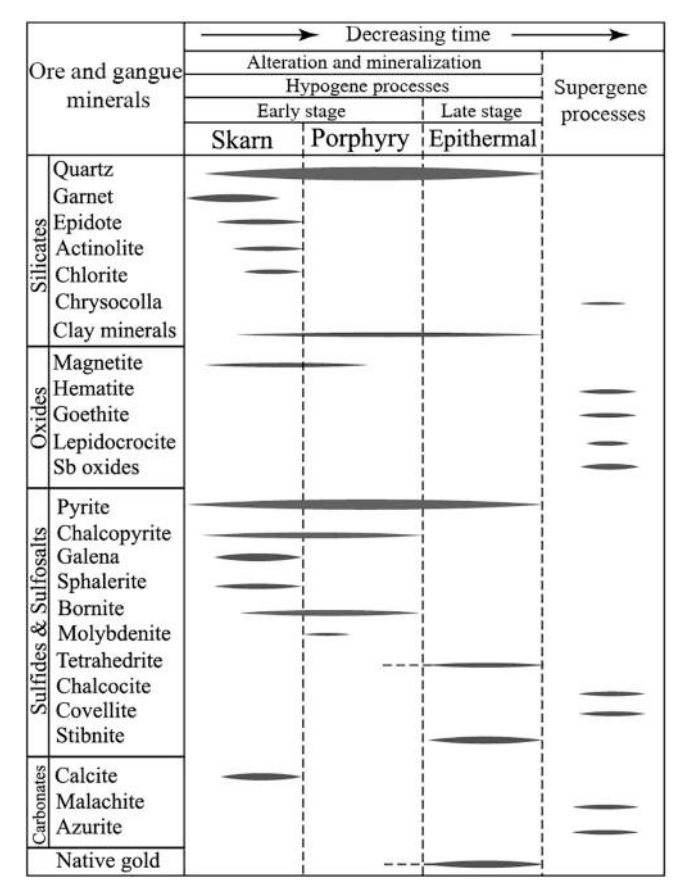


Fig. 7. Paragenetic sequence of metasomatic, porphyry and epithermal mineralizations, as well as later-stage supergene alteration, showing the temporal relationship between the mineral assemblages formed during alteration and mineralization processes in the Astarghan deposits.

show negative crystal, spindle and ellipsoid shapes. Primary inclusions have almost uniform distribution along the crystal growth surfaces, while secondary and pseudo-secondary fluid inclusions are aligned along the sealed fractures and have smaller sizes. However, the secondary ones are more abundant. Necking-down and leakage cases do also exist.

Based upon phase content, five types of fluid inclusions were recognized in the potassic alteration zone at Kaghdara: (1) mono-phase vapor (Fig. 8a), (2) vapor-rich 2-phase (V + L) (Fig. 8b), (3) liquid-rich 2-phase (L + V) (Fig. 8c), (4) halite-bearing multiphase (Fig. 8d), and (5) multi-solid (halite + sylvite + opaque daughter minerals) inclusions (Fig. 8e).

Quartz veinlets from the phyllic zone at Sildirimdara contain tetrahedrite and vary in thickness from 3 to 5 cm. The studied fluid inclusions within quartz crystals in these veinlets were merely 2-phase liquid-rich and rarely mono-phase vapor types (Fig. 8f).

4.7.2. Petrography of fluid inclusions in epithermal veinlets at Nowrozkala Samples from the epithermal mineralization zone at Nowrozkala were collected from sulfide–sulfosalt–gold bearing quartz veins/veinlets, which trend toward NE and are 2–20 cm thick. Fluid inclusions within quartz crystals of these veins/veinlets are relatively less abundant compared to the above-mentioned veinlets of the porphyry system, and are mainly round and occasionally spindle and/or elongate in shape. Their size ranges from 5 to 20 μm , where primary inclusions are much larger than secondary and pseudo-secondary ones. Two types of primary fluid inclusions are present within these veinlets: (1) liquid-rich 2-phase (L + V), being relatively abundant (Fig. 8g) and (2) mono-phase vapor. Some of liquid-rich 2-phase ones also show necking-down and/or

leakage features (Fig. 8h).

4.7.3. Microthermometric analysis on porphyry veinlets

Microthermometric studies on the quartz veinlets from potassic alteration zone at Kaghdara (n = 114; Table 1) showed that almost all of the 2-phase liquid-rich fluid inclusions were homogenized into liquid state and the 2-phase vapor-rich ones into vapor state during heating. However, the halite-bearing multiphase inclusions were also abundant in this zone and on heating, the majority of them were homogenized by halite dissolution ($T_{S(NaCl)} > T_{H(L-V)}$), although a small number of them were homogenized by vapor ($T_{S(NaCl)} < T_{H(L-V)}$) and simultaneous vapor–halite ($T_{S(NaCl)} = T_{H(L-V)}$) disappearance.

The overall frequency distribution of all 2-phase liquid-rich inclusions homogenizing into liquid state (Fig. 9a) shows a wide range of $T_{H(L-V)}$ values from 168 to 418 °C, while homogenization into vapor state of 2-phase vapor-rich inclusions occurs at temperatures of 228 to 460 °C (Fig. 9b). The halite-bearing inclusions homogenizing by halite disappearance ($T_{S(NaCl)} > T_{H(L-V)}$) display a wide range of $T_{S(NaCl)}$ values from 320 to 578 °C (Fig. 9c).

The overall salinity of the studied fluid inclusions in this zone varies from 5 to 69.3 wt% NaCl $_{\rm eq}$ (Fig. 9d). In this regard, liquid-rich 2-phase inclusions have the range of 160–420 $^{\circ}$ C, while vapor-rich 2-phase inclusions show a little higher temperatures of 220–460 $^{\circ}$ C, and the multiphase inclusions display much higher temperatures of 325–580 $^{\circ}$ C.

The prevalent liquid-rich 2-phase fluid inclusions from the quartz veins/veinlets of the phyllic alteration zone at Sildirimdara (n = 31) were homogenized into liquid state during heating. The $T_{H(L\cdot V)}$ values are about 175–345 °C (Fig. 9e), mainly clustering between 180 and 300 °C, and their salinity values range from 5.0 to 8.0 wt% NaCleq. (Fig. 9f).

4.7.4. Microthermometric analysis on epithermal veinlets

Microthermometric analysis on quartz veinlets from epithermal mineralization and the related argillic alteration zone at Nowrozkala (n = 103; Table 1) showed that all of the 2-phase fluid inclusions were homogenized into liquid state during heating. Their $T_{H(L-V)}$ values range from 118 to 325 °C (Fig. 9g), and their salinities lie within the range of 0.6 to 7.4 wt% NaCleq. (Fig. 9h).

4.7.5. Density of fluid inclusions in porphyry and epithermal veinlets

Densities of the halite-bearing multiphase and 2-phase fluid inclusions in quartz veinlets from the potassic alteration zone at Kaghdara lie within the ranges of $0.95-1.2 \text{ g/cm}^3$ and $0.6-1.0 \text{ g/cm}^3$, respectively, whereas density values of liquid-rich 2-phase fluid inclusions in quartz veins/veinlets from the phyllic alteration zone at Sildirimdara are between 0.7 and 0.9 g/cm^3 (Fig. 10a). Densities of 2-phase fluid inclusions in quartz veinlets from the epithermal mineralization at Nowrozkala are $< 1 \text{ g/cm}^3$, mainly clustering between 0.85 and 0.95 g/cm^3 (Fig. 10a).

4.8. Sulfur stable isotopes

The δ^{34} S values were measured on four pyrite separates from porphyry-type quartz–pyrite–chalcopyrite stockwork veinlets in the potassic alteration zone at Kaghdara, and epithermal quartz–sulfide–gold veinlets in the argillic zone at Nowrozkala (two samples from each type of veinlets; Table 2). Due to the fine-grained intergrowth and/or the presence of fine inclusions of other sulfides as impurities within chalcopyrite, sphalerite and galena, as well as their marginal supergene alterations, obtaining pure separates of these sulfides were not possible. On the other hand, since the δ^{34} S data from the skarn zone and porphyry mineralization in this deposit was previously published (Arjmandzadeh and Alirezai, 2005; Einali and Alirezai, 2005; will be discussed in section 5.3), no samples were analyzed from the skarn zone and only 2 supplementary analyses were performed for the porphyry mineralization in order to compare the results with the published data.

The measured δ^{34} S values on pyrites vary from-0.1% to -0.3% at

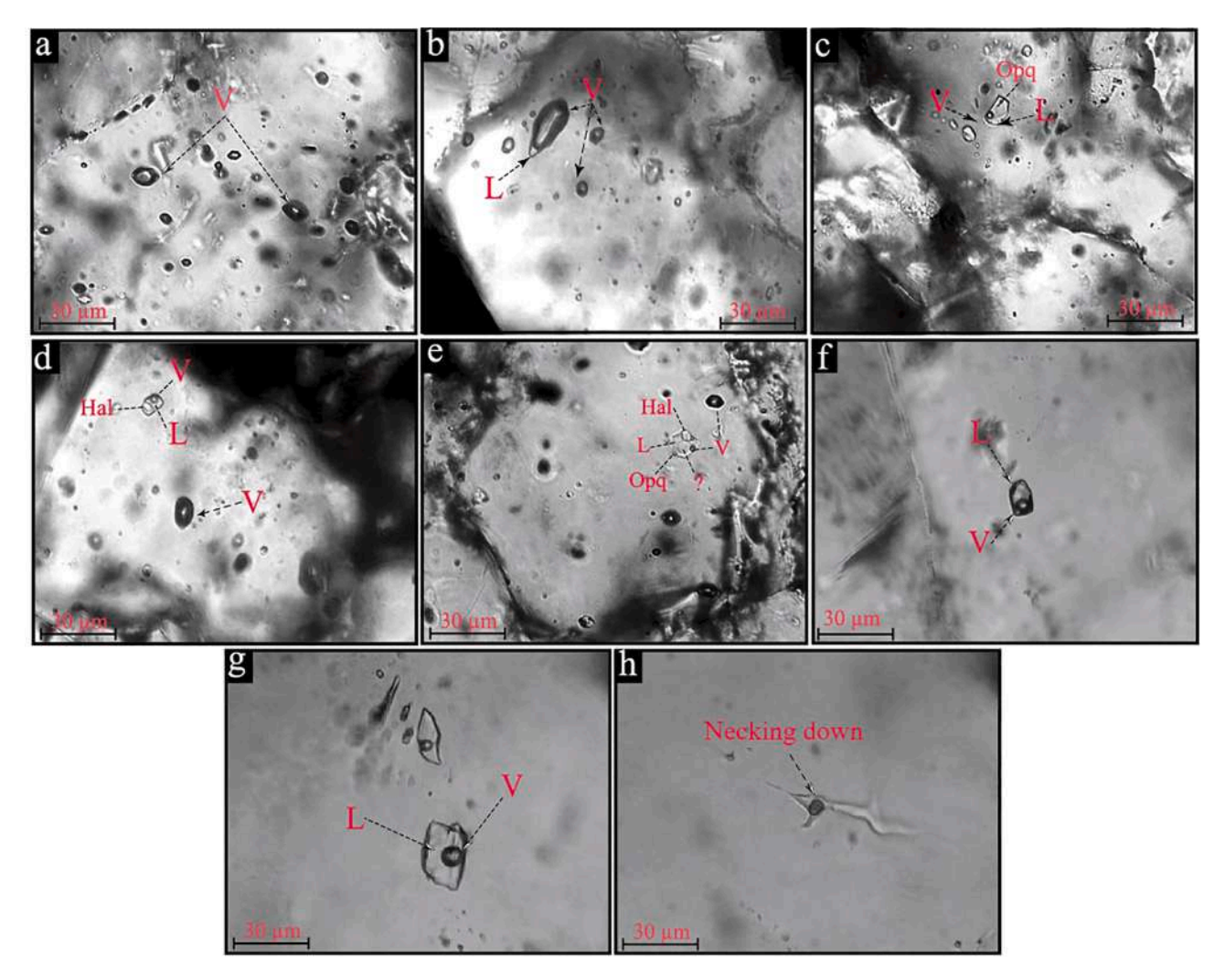


Fig. 8. Photomicrographs of various types of fluid inclusions within the quartz veins/veinlets (a–e from porphyry-type potassic alteration zone at Kaghdara). (a) Mono-phase vapor. (b) Vapor-rich 2-phase. (c) Halite-bearing multiphase together with a mono-phase vapor inclusion. (d) Liquid-rich 2-phase and a multiphase inclusion with an opaque daughter mineral. (e) A multi-solid inclusion containing an opaque and unknown daughter mineral, besides halite. (f) Liquid-rich 2-phase inclusion in a quartz vein at the porphyry-type phyllic alteration zone at Sildirimdara. (g) Liquid-rich 2-phase inclusions in a gold-bearing epithermal quartz vein at Nowrozkala. (h) Necking down in 2-phase inclusions of epithermal veins.

Kaghdara, and from -0.5% to -1.1% at Nowrozkala. The calculated δ^{34} S values for H_2 S in the mineralizing fluids range from -0.7% to -1.1% at Kaghdara and from -2.1% to -2.7% at Nowrozkala.

4.9. Mineral chemistry

In order to determine the gold content in each type of mineralization, the EPMA analysis was performed on sulfide minerals from skarn, porphyry and epithermal mineralizations (see Table 3 for the results). In the case of the porphyry system, pyrite, chalcopyrite (from stockwork veinlets of the Kaghdara potassic zone) and tetrahedrite (from quartz—tetrahedrite veinlets of the Sildirimdara phyllic zone) were analyzed as the dominant hypogene sulfides. From the epithermal mineralization zone, pyrite, stibnite and native gold particles were analyzed. For the skarn zone, only galena was analyzed, as this mineral was not found within the other mineralized zones.

4.9.1. Skarn zone

Galena: The analyzed galena particles from the exoskarn zone had no Au and Ag. However, they showed high concentrations of W (0–0.19 wt %), Bi (0.21–0.94 wt%) and Te (0.03–0.15 wt%). The average Sb/Bi ratio is about 0.21. The average chemical composition of galena

incorporates 78.72% Pb and 15.13% S.

4.9.2. Porphyry system

(a) Pyrite: The analyzed pyrite grains from the quartz–sulfide veinlets of the porphyry mineralization zone showed no Au and Ag content (except for one sample containing 100 ppm Ag). However, these pyrites are characterized by high Cu contents, up to 1 wt%, with an average of 0.35 wt%.

The average concentration of As in pyrites is about 0.12 wt%, though high concentrations up to 0.72 wt% have also been measured. Ni and Zn also show maximum concentrations of 4300 and 1100 ppm. The highest contents of Hg, Bi and Te within the pyrites are 1100, 3300 and 1000 ppm, respectively. The average of major elemental components in this mineral is 46.33 wt% Fe and 52.85 wt% S.

(b) Chalcopyrite: The average contents of Cu, Fe and S in the analyzed chalcopyrite grains from the porphyry mineralization zone are 36.9, 27.6 and 31.1 wt%, respectively, and the calculated mineral formula is Fe_{1.1}Cu_{0.9}S₂.The highest gold content is 800 ppm, with an average of 290 ppm. Among the trace elements, Ag, Sb and As have relatively high concentrations, with peak values of 400 ppm, 300 ppm and 300 ppm, respectively.

(c) Tetrahedrite-Tenantite: The gold content of tetrahedrite grains

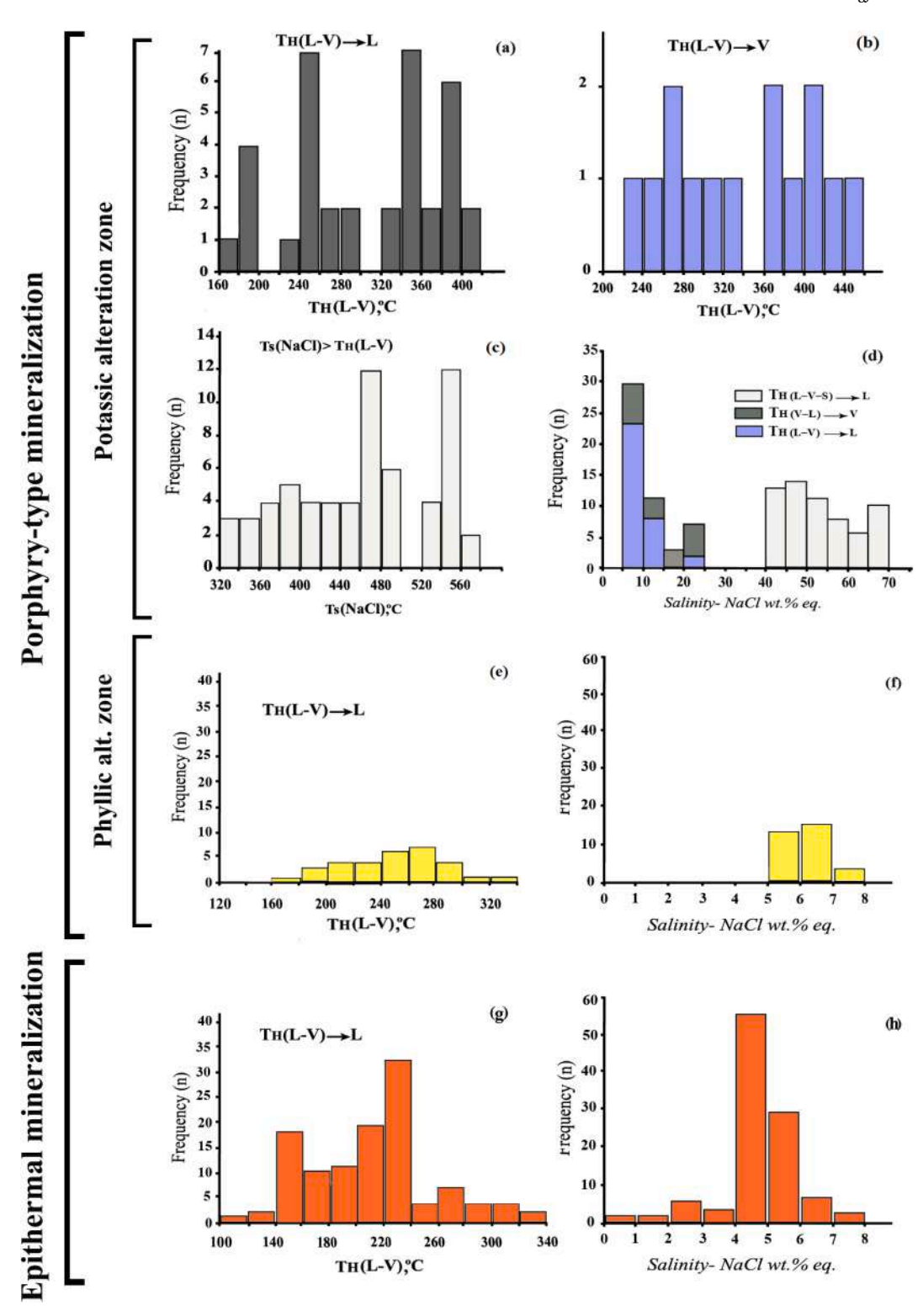


Fig. 9. Histograms of homogenization temperatures ($T_{H(L-V)}$) and salinities of the studied fluid inclusions. (a) $T_{H(L-V)}$ for liquid-rich 2-phase inclusions homogenizing into liquid state (Kaghdara). (b) $T_{H(L-V)}$ for vapor-rich 2-phase inclusions homogenizing into vapor state (Kaghdara). (c) $T_{S(NaCl)}$ for halite-bearing inclusions with $T_{S(NaCl)} > T_{H(L-V)}$ (Kaghdara). (d) Frequency distribution of salinities for the quartz veins/veinlets of the porphyry-type potassic zone at Kaghdara. (e) $T_{H(L-V)}$ values for the phyllic alteration zone at Sildirimdara. (g) $T_{H(L-V)}$ values from epithermal veins at Nowrozkala. (h) Salinity values of the studied fluid inclusions from epithermal veins at Nowrozkala.

ranges from 100 to 6400 ppm, with an average of 1300 ppm. This mineral (as solid solution series) is also rich in As (0.7-18.9 wt%), with an average of 6.3 wt%), Ag (0.05-1.59 wt%) with a mean value of 6230 ppm) and Te (0.02-3.51 wt%), with a mean of 4780 ppm). The calculated chemical formula for this mineral is $(Cu_{9.36}Pb_{0.26}Zn_{1.04})(As_{1.04}Sb_{2.6})S_{13}$.

4.9.3. Epithermal system

(a) Pyrite: The EPMA results of pyrite grains from the epithermal mineralization zone showed a gold content up to 500 ppm (measured on an automorphic and polyhedral pyrite grain), while the Ag content is up to 200 ppm. Furthermore, the majority of the analyzed pyrites showed

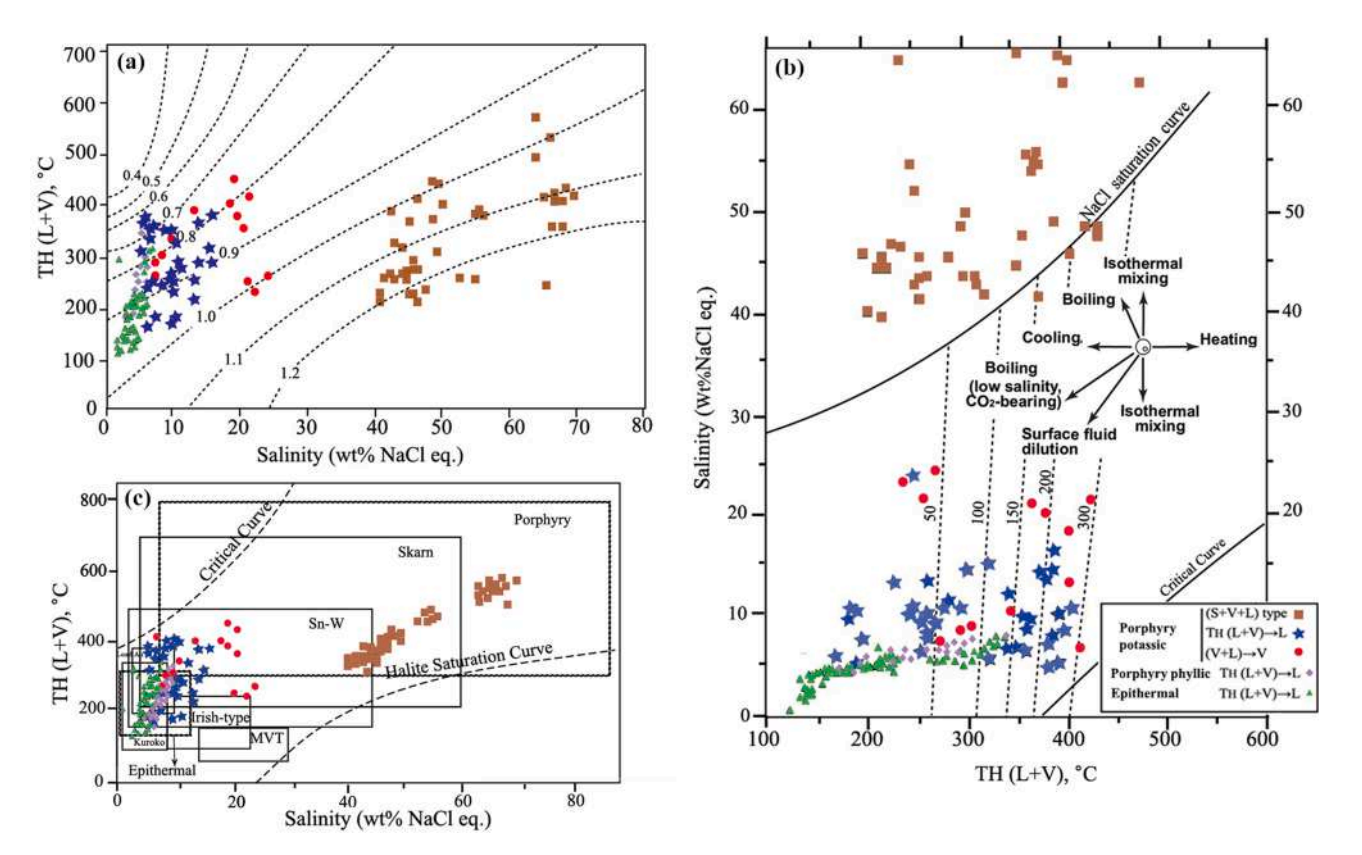


Fig. 10. Plots of $T_{H(L-V)}$ versus salinity showing (a) density values (g/cm³) of the fluid inclusions from porphyry-type potassic and phyllic alteration zones and epithermal mineralization; (b) the distribution of data points from porphyry and epithermal zones [the NaCl saturation and critical curves are from Ahmad and Rose (1980) and the dashed lines related to vapor pressures of NaCl solutions are from Roedder (1984)]; (c) salinity and temperature ranges of different types of hydrothermal deposits (Wilkinson, 2001).

no Cu content (except for one point with 800 ppm Cu). The highest contents of Hg, Bi, Te and As within the pyrites are 2100, 1600, 400 and 300 ppm, respectively. Zn and Ni contents are also below 500 and 100 ppm, respectively. The averages of iron and sulfur contents in the analyzed pyrites are 47.10% and 52.78%, respectively.

(b) Stibnite: The Sb content of the analyzed points on stibnites ranges from 61.22 to 70.05 wt%, with an average of 65.23 wt%, while they also contain an average of 20.37 wt% sulfur (16.28-24.30 wt%). The gold content of the analyzed stibnite grains ranges from 6.07 to 12.00 wt%, with an average of 9.50 wt%. This mineral also hosts high contents of As (2.50-4.32 wt%; average of 3.26 wt%) and Hg (0.01-4.09 wt%; average of 1.08 wt%), but is mostly Ag-free, except for one point which showed 400 ppm concentration.

(c) Native gold: Native gold is found in quartz-stibnite epithermal veins/veinlets, along with sulfide (especially pyrite). It contains 94.70 wt% Au and 2.19 wt% Ag on average (93.6–96.5 wt% and 0.15–3.90 wt%, respectively), while the mean value of Bi is 260 ppm and one point yielded 800 ppm Cu.

5. Discussion

5.1. Evolution of the skarn-porphyry-hydrothermal system

5.1.1. Skarn formation

Intrusion of the Oligo–Miocene Astarghan porphyry stock (granodioritic to quartz-monzonitic) into the upper Cretaceous–Paleocene flyschtype sequence induced enormous heat flow in the host rocks and brought about extensive fracturing and ensuing hydrothermal activities. The heat and hydrothermal fluids resulted in metamorphism and development of metasomatic alterations along the contact zone. The porphyrytype copper mineralization and related hydrothermal alterations were

taken place within the porphyry intrusive stock by magmatic-hydrothermal fluids, followed by the late-stage epithermal sulfi-de-sulfosalt-gold mineralization in the area.

Based upon field observations and petrographic studies, the evolutionary sequence of the Astarghan deposit can be described as follows: during the prograde stage of skarn formation, anhydrous calc-silicate minerals were formed by metamorphic-bimetasomatic and metasomatic processes. The metamorphic-bimetasomatic sub-stage was contemporaneous with the emplacement of the intrusive body, and the heat flow originated from it caused isochemical metamorphism in the country rocks. In addition to the formation of contact metamorphic rocks such as marble, hornfels and metapelite within the host rocks, intercalations of siltstone and sandstone within the host carbonate rocks served as a source for Si, Al and Mg, leading to the formation of finegrained isotropic garnet and pyroxene in proximity of the contact zone and epidote within the distal zones. Moreover, occurrence of decarbonation reactions within the host carbonate rocks caused slight volume loss, manifested by the formation of fractures and joints within the country rocks, paving the ground for the later stages of skarnification. Element transfer was not occurred in this stage, except for volatiles.

The metasomatic sub-stage is characterized by the formation of garnet-skarn zone in the vicinity of the contact zone, most likely after the partial solidification of the intrusive body and evolution of the hydrothermal fluids and their penetration into the country rocks. This led to the formation of coarse-grained anhydrous calc-silicates (e.g., garnet and pyroxene) within the exoskarn zone. On the other hand, formation of metasomatic minerals in the endoskarn zone is resulted from mutual diffusion of elements between the intrusive body (hydrothermal fluids) and the country rocks and the introduction of Ca into the stock. Garnets crystallized in this sub-stage are coarser than the previous sub-stage and locally show overgrowth with the earlier ones. Microthermometric

analysis on some fluid inclusions within the garnet crystals indicates higher temperatures for fluids of this stage, as they did not homogenize even at 600 $^{\circ}$ C. The presence of wollastonite in the banded skarn samples also confirms that the formation of prograde-stage anhydrous calc-silicates occurred at $>550~^{\circ}$ C.

However, the ensuing retrograde stage was accompanied by some physico–chemical changes (decrease in temperature, increase in fS_2 , incorporation of meteoric waters) that altered the pre-existing anhydrous calc-silicates (garnet, pyroxene) to hydrous calc-silicates (epidote, and tremolite–actinolite), silicates (quartz, chlorites, and other clay minerals), along with the formation of oxides (magnetite and hematite), sulfides (pyrite, chalcopyrite, galena and sphalerite), and carbonates (calcite). This mineral assemblage must be formed at temperatures of < 400 $^{\circ}$ C (Rose and Burt, 1979), which is confirmed by the fluid inclusion microthermometry data. Ubiquitous replacement and open-space filling textures of opaque minerals in the exoskarn zone signify that most of them have been precipitated during the early retrograde stage.

The scarcity of garnet (especially in the massive exoskarn) and the conversion of clinopyroxene to tremolite-actinolite in the exoskarn zone at Astarghan further confirm the reactions occurred during retrograde stage at lower temperatures (Einaudi et al., 1981). Furthermore, replacement by calcite-quartz-magnetite assemblage is an important retrograde reaction which occurred in andradite-rich skarns at relatively low-sulfidation conditions (Bean, 1982). Hence, the presence of this assemblage in the studied skarn may indicate the composition of primary garnets and its sulfidation state. Finally, the higher content of actinolite compared to tremolite in the studied skarn samples from Astarghan also testifies that the composition of clinopyroxenes formed at the metasomatic sub-stage was mainly hedenbergite (Einaudi et al., 1981).

5.1.2. Porphyry mineralization and the associated hydrothermal alterations Skarn zones at Astarghan are intimately associated with the porphyry stock. The main part of the skarn mineralization is found at Kaghdara, in the vicinity of potassic alteration zone of the porphyry system. During the metamorphic-bimetasomatic stage, the prevalent pressure is lithostatic, whereas the prograde metasomatic stage requires fractures and paths for fluid flow. Development of the porphyry mineralization and especially potassic alteration-mineralization zone (cropped out at Kaghdara) also requires fracturing under hydrostatic pressure. In this regard, it can be perceived that the potassic zone and the prograde metasomatic alteration in Kaghdara were almost coeval. Meinert et al. (2003) have also stated that the prograde mineral assemblage in Ca-skarns is formed contemporaneously with the potassic alteration zone within the porphyry stocks, while the retrograde assemblage of hydrous calc-silicates, oxides and sulfides are formed coeval with the phyllic-sericitic alteration in the porphyry systems.

5.1.3. Epithermal mineralization

The epithermal mineralization in the Astarghan represents the youngest mineralization phase, which is developed within the intensely altered (argillic) granodiorite to quartz-monzonite porphyry stock at higher elevations in the Nowrozkala area, about 1000 m higher compared to the potassic zone at Kaghdara. Porphyry deposits are potential sources for gold mineralization but the highest grades of precious metals are limited to epithermal veins/veinlets (Arribas et al., 1995; Jannas et al., 1990). Porphyry and epithermal deposits occur spatially and also temporally related to each other (Arribas et al., 1995), which indicates the common source of ore-forming fluids in these deposits. Fluid inclusion studies on samples from the porphyry and epithermal veinlets at Astarghan show the evolution of hydrothermal fluids from high-temperature and high-salinity fluids to low-temperature and low-salinity ones, caused by cooling and mixing with meteoric waters as they ascend from depth, which will be discussed in the next section.

Epithermal quartz veins/veinlets in this deposit contain higher gold content. Following the occurrence of boiling event, the H₂S-bearing

ascending vapor phase from K-rich rocks of the potassic zone provides an essential tool for optimal transportation of gold from porphyry to epithermal system as bisulfide complexes (Seward and Barnes, 1997). Neutralization of the acidity of fluids following the destruction of feldspars within the phyllic and argillic alteration zones facilitates the gold transportation as Au(HS) from porphyry towards the epithermal zones (Heinrich, 2005). Finally, the temperature and pressure decline and oxidation of the fluids lead to a decrease in the sulfur activity and precipitation of sulfides along with gold in the epithermal veins/veinlets.

Finally, taking into account the evidence such as the lack of enargite and luzonite (characteristic of high-sulfidation mineralization), lack of vast advanced argillic alteration, the presence of gold and to lesser extent Ag, the occurrence of boiling as the main factor for ore precipitation, the low salinity of ore-forming fluids at epithermal stage and their mixing with meteoric waters (see section 5.2), the ubiquitous open-space filling and drusy textures of the epithermal veins/veinlets (Hedenquist et al., 1998), the substantial gold mineralization in the Astarghan was classified as epithermal-type with low-sulfidation nature.

5.2. Interpretation of the fluid inclusion data

Two populations of high-salinity (halite-bearing multiphase) and moderate to low-salinity (2-phase) fluid inclusions were recognized within stockwork veinlets of the potassic alteration zone in the porphyry mineralization system. The general trend of each dataset corresponds well with a boiling event (Fig. 10b). Moreover, the coexistence of monophase vapor, 2-phase vapor-rich, 2-phase liquid-rich, and halite-bearing multiphase fluid inclusions homogenizing over the same temperature range (220–460 °C) within the quartz veinlets of the potassic alteration zone at Kaghdara may also confirm that the ore-bearing fluids underwent boiling (Nash, 1976; Bodnar and Vityk, 1994; Hedenquist et al., 1998). Such coexistence of monophase-vapor, 2-phase and multiphase fluid inclusions have been reported from other porphyry Cu deposits worldwide and especially from Sungun (Calagari, 2003) and Kighal (Simmonds et al., 2015) PCDs, NW Iran.

The boiling events and concurrent hydraulic fracturing can be reasonably verified by the presence of numerous cross-cutting veinlets and stockwork structures in this zone. Furthermore, the wide range of salinity values (Figs. 9, 10b) due to the coexistence of 2-phase (liquid-and vapor-rich) and halite-bearing multiphase inclusions homogenizing over the same temperature range, their various volume fractions and the presence of mono-phase vapor inclusions may also confirm the boiling of ore-bearing fluids and separation of a high-salinity liquid phase from a low-salinity vapor-rich phase, following the initial separation of an aqueous phase from magma at pressures below 1.3 kb (Den Kerkhof and Hein, 2001; Wilkinson, 2001) rather than direct segregation of a saline fluid from crystallizing magma (Roedder, 1978).

On the other hand, the $T_{H(L-V)}$ and salinity values obtained for fluid inclusions in the quartz veinlets from the Sildirimdara phyllic zone may reflect a temperature decrease in the hypogene ore-bearing fluids, as they ascended to higher levels (shallower depths) and were probably mixed with groundwaters of meteoric origin (Fig. 10b).

Fluid inclusions within the epithermal quartz veinlets of the Nowrozkala are characterized by low $T_{H(L\cdot V)}$ and salinity values, and show a decreasing trend for temperature, probably due to cooling and mixing with groundwaters and descending surficial fluids.

Based on the bivariate plot of salinity versus $T_{H(L-V)}$ (Fig. 10b), the various types of fluid inclusions from porphyry and epithermal veinlets in the Astarghan can be categorized as follows:

1. The halite-bearing multiphase fluid inclusions with $T_{S(NaCl)} > T_{H(L-V)}$, which lie above the halite saturation curve. These only occur in the potassic alteration zone at Kaghdara and it seems that these inclusions have trapped NaCl-supersaturated fluids or even solid halite crystals.

- 2. The halite-bearing multiphase inclusions with $T_{S(NaCl)} < T_{H(L-V)}$ and $T_{S(NaCl)} = T_{H(L-V)}$, lying below and on the halite saturation curve, which are thought to trap near-saturated and almost saturated (with respect to NaCl) fluids. These also belong to the Kaghdara potassic zone
- The 2-phase fluid inclusions from the Kaghdara potassic zone, which have rather moderate salinity and homogenization temperatures, especially the vapor-rich inclusions.
- 4. The 2-phase fluid inclusions with low salinity and low homogenization temperatures from the Sildirimdara phyllic zone, which plot lower than the same fluid inclusions from the Kaghdara potassic zone.
- 5. Finally, the low salinity and low temperature 2-phase fluid inclusions from the epithermal veinlets at Nowrozkala, which overlap with the 2-phase inclusions of the Sildirimdara phyllic zone at the salinity and temperature range of 5.0–7.4 wt% NaCleq. and 160–325 $^{\circ}\text{C}$, respectively, but also display much lower values.

According to the salinity vs. $T_{H(L-V)}$ plot in Fig. 10c, data points of the Kaghdara potassic zone fall in the porphyry field, while those of the Nowrozkala epithermal veinlets lie within the epithermal field. The data points of the Sildirimdara phyllic zone plot within both porphyry and epithermal fields.

According to the $T_{H(L-V)}$ range (118–325 °C) and salinity values (0.6–7.4 wt%) in the Nowrozkala epithermal veinlets, the minimum estimated pressures at the time of entrapment of the ore-bearing fluids were estimated to be within the range of 20–100 bar, which correspond to the depths of 180–900 m below the underground water table. Similarly, on the basis of $T_{H(L-V)}$ (168–418 °C) and salinity (5–23.5 wt%) values obtained for 2-phase fluid inclusions of the Kaghdara potassic zone, the minimum hydrostatic pressure experienced by the ore-bearing fluids at the time of entrapment was estimated to be within the range of 25–280 bars, which corresponds to depths within the range of 225–2520 m below the underground water table. The minimum pressure estimated for Sildirimdara phyllic alteration zone is also < 150 bars, being intermediate compared to potassic and epithermal zones.

The estimated pressures for the halite-bearing multiphase fluid inclusions from the porphyry-type potassic alteration zone, whose T_{H(L-V)} values are close or almost equal to T_{S(NaCl)}, are within the range of 180-250 bars, equivalent to hydraulic heads of 1620-2250 m. Those fluid inclusions with T_{S(NaCl)} values higher than T_{H(L-V)} show a pressure range of 930-2350 bars, which corresponds to hydraulic heads of 3-8.2 km. On this basis, there is a big pressure difference between two series of coexisting fluid inclusions in quartz-sulfide veinlets of Kaghdara potassic zone. In fact, it seems to be rather unrealistic that any single quartz crystal could trap several fluids at enormously different hydrostatic pressures. Therefore, it is conceivable that fluid inclusions having $T_{S(NaCl)} > T_{H(L-V)}$ do not represent the actual salinity of the boiling fluids. These inclusions might have trapped tiny suspended halite crystals from the boiling supersaturated fluids (e.g., Calagari, 2003; Chi et al., 2017) and/or formed by the necking-down of the trapped inclusions (Ahmad and Rose, 1980; Gultekin and Balci, 2016). Finally, the approximate depth of the porphyry mineralization, regardless the false pressures mentioned above, ranges from 1.6 to 2.5 km, whereas the estimated depth of the epithermal mineralization is < 0.9 km.

5.3. Interpretation of S isotope data

The measured $\delta^{34}S$ values of pyrite separates from the Kaghdara porphyry (–0.1 to –0.3‰) and Nowrozkala epithermal mineralizations (–0.5 to –1.1‰), as well as the calculated $\delta^{34}S$ values for H_2S in the mineralizing fluids (–0.7 to –1.1‰, and –2.1 to 2.7‰, respectively) reasonably suggest a magmatic source for sulfur, which is thought to be derived directly from magma underneath and/or leaching from pre-existing sulfides (Hoefs, 2004) in the enclosing igneous rocks.

To these must be added the S isotope data reported by Einali and

Alirezai (2005) for pyrite from the massive and banded skarn, which range from -2.7 to -0.1‰ and -0.7 to 0.4‰, respectively. These data also lie within the field of magmatic origin. Moreover, Arjmandzadeh and Alirezai (2005) analyzed 10 samples of pyrite, chalcopyrite and bornite from quartz veins within the potassic and phyllic alteration zones of the porphyry stock, the results of which range from -2.8 to 1.0‰, showing overlap with the results of this research and further indicate a magmatic origin.

It must be added that the measured $\delta^{34}S$ values of pyrite from the porphyry veinlets in this research are higher than those in epithermal veinlets. This difference can be attributed to the precipitation of the main part of heavy S isotopes during the porphyry mineralization, while ^{32}S isotopes have remained within the fluid until the epithermal mineralization at lower temperatures, leading to lighter $\delta^{34}S$ values in sulfides of this stage.

In comparison with some neighboring Cu (Mo–Au) deposits such as Sungun (–4.6 to –0.2‰; Calagari, 2003), Kighal (–0.1 to 1.3‰; Simmonds et al., 2015), Qarachilar (–0.8 to 0.5‰; Simmonds et al., 2016) porphyry deposits and Zailic-Sarilar (–2.3 to 1.8‰; Miranvari et al., 2020) epithermal mineralization, the $\delta^{34}S$ values of sulfides share common ranges (Fig. 11).

The low abundance of sulfates merely within the diamond-drill cores of the potassic alteration zone (anhydrite and gypsum), and the predominance of sulfides (especially pyrite), as well as the negative values of $\delta^{34} S$ indicate that ore bearing fluids had relatively low pH and fO_2 values (Ohmoto and Rye, 1979). This results in low mole fraction of SO_2 at higher temperatures and/or $SO_2^{2^+}$ at lower temperatures within the fluids and therefore, H_2S species was prevailing during the sulfide precipitation. Furthermore, processes such as boiling (as evidenced by fluid inclusion data) and removal of enormous quantity of H_2S as an exsolved volatile and/or sulfide minerals from the fluid phase presumably increased the $SO_4^{2^+}$ to H_2S (aq.) ratio in the fluid (Ohmoto and Rye, 1979) during the waning stage of the sulfide mineralization.

5.4. The EPMA data interpretation

The EPMA data along with detailed stoichiometry of the analyzed ore minerals resulted in more accurate identification of gold-hosting minerals. According to the obtained results, gold content in the porphyry-related chalcopyrite reaches up to 800 ppm (mean of 260 ppm), while pyrites in this zone have no Au. However, tetrahedrites within the quartz veins of phyllic alteration zone contain high gold content, up to 0.64 wt %

In the epithermal mineralization, gold is associated with stibnites

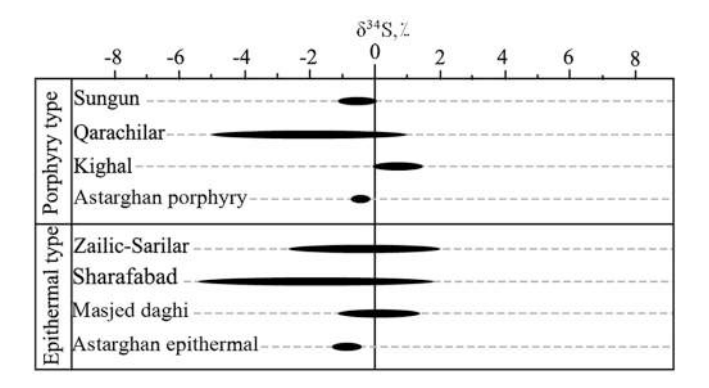


Fig. 11. The δ^{34} S values of the pyrite separates from the porphyry-type potassic alteration zone at Kaghdara and the epithermal mineralization at Nowrozkala, compared to the δ^{34} S values of sulfides from other porphyry and epithermal occurrences in the Arasbaran metallogenic zone. The δ^{34} S values of Sungun from Calagari (2004b), Qarachilar from Simmonds et al. (2016), Kighal from Simmonds et al. (2015), Zailic-Sarilar from Miranvari et al. (2020), Sharafabad from Radmard et al. (2017) and Masjed Daghi from Ebrahimi et al. (2017).

(6.07 to 12 wt%) and automorphic polyhedral pyrite grains (up to 500 ppm); petrographic studies also showed the presence of native gold inclusions within these grains. Stibnites in this zone have the highest gold content; even the associated antimony oxides contain gold particles. Meanwhile, the low Sb values of about 61.22 to 70.05 wt% in stibnites are probably due to their oxidation in the surface outcrops.

In this regard, low-temperature sulfosalts (tetrahedrite-tenantite) and sulfide (especially stibnite) minerals, respectively within the porphyry and epithermal quartz veinlets yielded higher Au contents (averages of 0.13 and 9.5 wt%, respectively) and were recognized as the main hosts for gold in the Astarghan deposit.

The presence of native gold inclusions within stibnite led us to the deduction that deposition of natural gold was coeval with the crystallization of stibnite from an epithermal fluid following the breaking down of the bisulfide complexes.

Galena from the exoskarn zone showed no Au content and moreover, BSE images didn't show any gold particle within the sulfide minerals of exoskarn zone. The Sb/Bi ratio of about 0.21 in galena indicates its formation at later-stage low temperatures (Song, 1984).

6. Conclusions

Based on field observations, petrographic studies and microthermometric, sulfur isotope and EPMA analyses, the following conclusions were drawn for the gold mineralization in the Astarghan deposits:

- 1) Intrusion of the Oligo–Miocene Astarghan porphyry stock (granodioritic to quartz-monzonitic) into the upper Cretaceous flysch-type sequence, along with the induced heat and the evolution of hydrothermal fluids derived from it brought about base metal (Cu–Pb–Zn) skarn alteration and mineralization at the contact of flysch-type host rocks (particularly the impure carbonates), the Cu–Au porphyry mineralization and related hydrothermal alterations within the porphyry stock, and the gold–stibnite low-sulfidation epithermal mineralization hosted by argillic alteration halo within the porphyry stock.
- 2) Native gold inclusions are present within or around the automorphic polyhedral pyrites, stibnites and antimony oxides of the epithermal veins/veinlets, within the tetrahedrites in the porphyry-type phyllic alteration zone at Sildirimdara, as well as within the epithermal quartz veins/veinlets, where they appear as separate tiny particles of $50-200~\mu m$.
- 3) Microthermometric studies showed that porphyry mineralization includes 2 populations of high-salinity (multiphase) and moderate to low-salinity (2-phase) fluid inclusions. However, fluid inclusions within the epithermal veinlets (2-phase) have lower salinity and temperature compared to porphyry-related ones. The evolution of hydrothermal fluids from skarn zone (high temperature) towards the epithermal veinlets (low temperature) might have occurred by mixing of hot magmatic ascending fluids with relatively cool and low-salinity groundwaters of meteoric origin.
- 4) The isotopic composition of sulfur within both the porphyry and epithermal mineralization zones corresponds to the magmatic sulfur, being lower in epithermal sulfides compared to the porphyry system, which can be attributed to precipitation of heavy isotopes at higher temperatures during the porphyry mineralization.
- 5) The EPMA analyses indicate that relatively low-temperature sulfosalts (tetrahedrite-tenantite) and sulfide (stibnite) minerals, respectively from the porphyry and epithermal systems, are the main hosts for gold in the Astarghan deposits. Petrographic examinations together with BSE images demonstrated that native gold occurs as inclusions within tetrahedrite-tenantite and stibnite crystals, as well as within or adjacent to the polyhedral pyrites, and also as separate minute particles within the epithermal quartz veins/veinlets.

6) The base-metal sulfides and gold mineralization at Astarghan is similar to those found in the neighboring areas (e.g., Sungun and Kighal porphyry Cu–Mo and the Masjed Daghi Cu–Au deposits) in terms of age, host rocks, alteration and mineralization style, and characteristics of the fluid inclusions. However, the existence of three distinct types of skarn (Cu–Pb–Zn), porphyry (Cu–Au) and low-sulfidation epithermal (Au–Sb) mineralizations in the Astarghan area makes it rather peculiar in NW Iran.

Declaration of Competing Interest

The authors declare that they have no known competing financial interests or personal relationships that could have appeared to influence the work reported in this paper.

Acknowledgements

This contribution is a part of the first author's PhD dissertation at the University of Tabriz. The authors would like to express their appreciation to the Research Deputy Bureau of the University of Tabriz for financial support, authorities of the Zarrin-Dagh-e-Astarkan Company for providing accommodation and logistic facilities, the Stable and Noble Gas Isotopes Laboratory of the University of Salamanca (Spain) for S isotope analysis, and the Iranian Mineral Research Center laboratory for geochemical and microthermometric analyses. Our appreciation is further expressed to Co-Editor-in-Chief of the journal, Prof. Pirajno, as well as the anonymous reviewers of the manuscript for making valuable comments and constructive suggestions on this manuscript.

References

- Agha Nabaty, E., 2004. Geology of Iran. Geological survey and mineral exploration organization of Iran, $586~\rm p.$
- Aghazadeh, M., Castro, A., Badrzadeh, Z., Vogt, K., 2011. Post-collisional polycyclic plutonism from the Zagros hinterland: the Shaivar Dagh plutonic complex, Alborz belt, Iran. Geol. Mag. 148, 980–1008.
- Aghazadeh, M., Hou, Z., Badrzadeh, Z., Zhou, L., 2015. Temporal-spatial distribution and tectonic setting of porphyry copper deposits in Iran: Constraints from zircon U–Pb and molybdenite Re–Os geochronology. Ore Geol. Rev. 70, 385–406.
- Ahmad, S.N., Rose, A.W., 1980. Fluid inclusions in porphyry and skarn ore at Santa Rita, New Mexico. Econ. Geol. 75, 229–250.
- Alavi, M., 1994. Tectonics of the Zagros orogenic belt of Iran: New data and interpretations. Tectonophys. 229, 211–238.
- Arjmandzadeh, R., Alirezai, S., 2005. The source of sulfur in sulfide minerals from various ore and alteration zones in Kharvana Cu-Au deposit, East Azarbaijan, NW Iran. Geological Survey of Iran, Tehran.
- Arribas, A.Jr., Hedenquist, J.W., Itaya, T., Okada, T., Concepción, R.A., Garcia, J.S.Jr., 1995. Contemporaneous formation of adjacent porphyry and epithermal Cu-Au deposits over 300 ka in northern Luzon, Philippines. Geol. 23, 337–340.
- Atalou, S., Nazafati, N., Lotfi, M., Aghazadeh, M., 2017. Fluid inclusion investigations of the Masjed Daghi copper–gold porphyry–epithermal mineralization, East Azerbaijan Province, NW Iran. Open J. Geol. 7, 1110–1127.
- Ayati, F., Yavuz, F., Asadi, H.H., Richards, J.P., Jourdan, F., 2013. Petrology and geochemistry of calc-alkaline volcanic and subvolcanic rocks, Dalli porphyry copper–gold deposit, Markazi Province, Iran. Int. Geol. Rev. 55, 158–184.
- Babazadeh, V.M., Makhmudov, A.I., Ramazanov, V.G., 1990. Porphyry copper and molybdenum deposits. Baku, Azerbaijan. Publication, 377 p. (in Russian with German and English abstracts).
- Bean, R.E., 1982. The magmatic–meteoric transition. Geothermal Resource Council Report 13, 245–253.
- $Bodnar, R.J., Vityk, M.O., 1994. \label{eq:hamiltonian} In: De Vivi, B., Frezzoti, M.L. (Eds.), Fluid inclusions in minerals, Methods and applications. Virginia Polytechnic Institute, Blacksburg.$
- Calagari, A.A., 2003. Fluid inclusion studies in quartz veinlets in the porphyry copper deposit at Sungun, East Azarbaidjan, Iran. J. Asian Earth Sci. 23, 179–189.
- Calagari, A.A., 2004a. Geology and fracture-related hypogene hydrothermal alteration and mineralization of porphyry copper deposit at Sungun. J. Geol. Soc. India 64, 595–618.
- Calagari, A.A., 2004b. Stable isotope (S, O, H and C) studies of phyllic and potassic-phyllic alteration zones of the porphyry copper deposit at Sungun, East-Azarbajian, Iran, J. Asian Earth Sci. 21, 767–780.
- Calagari, A.A., Hosseinzadeh, G.h., 2006. The mineralogy of copper-bearing skarn to the east of the Sungun-Chay river, Eastern Azarbaijan, Iran. J. Asian Earth Sci. 28, 423–438.
- Chi, G., Haid, T., Quirt, D., Fayek, M., Blamey, N., Chu, H., 2017. Petrography, fluid inclusion analysis and geochronology of the End uranium deposit, Kiggavik, Nunavut, Canada. Mineral. Depos. 52, 211–232.

- Den Kerkhof, V., Hein, U., 2001. Fluid inclusion petrography. Lithos 55, 27-47.
- Ebrahimi, S., Alirezai, S., Pan, Y., Mohammadi, B., 2017. Geology, mineralogy and ore fluid characteristics of the Masjed Daghi gold bearing veins system, NW Iran. J. Econ Geol. 9, 561–586 (in Persian with an extended English abstract).
- Einali, M., Alirezai, S., 2005. Source of sulfur in Mivehrood skarns and mineralized dykes, East Azarbaijan, NW Iran. Geological Survey of Iran, Tehran.
- Einaudi, M.T., Meinert, L.D., Newberry, R.J., 1981. Skarn deposits. Econ. Geol. 75, 317–391.
- Fatehi, M., Asadi, H.H., 2017. Application of semi-supervised fuzzy c-means method in clustering multivariate geochemical data, a case study from the Dalli Cu–Au porphyry deposit in central Iran. Ore Geol. Rev. 81, 245–255.
- Fatehi, M., Asadi, H.H., 2019. Geophysical signatures of gold rich porphyry copper deposits: A case study at the Dalli Cu–Au porphyry deposit. J. Econ. Geol. 10, 639–675 (in Persian with an English abstract).
- Ghorbani, M., 2013. The Economic Geology of Iran: Mineral Deposits and Natural Resources. Springer, p. 572 p..
- Gultekin, A.H., Balci, N., 2016. Mineralogy, geochemistry and fluid inclusion data from the Tumanpinari volcanic rock-hosted Fe–Mn–Ba deposit, Balikesir-Dursunbey, Turkey. Mineral. 6, 120.
- Hajalilou, B., Aghazadeh, M., 2016. Geological, alteration and mineralization characteristics of Ali Javad porphyry Cu-Au deposit, Arasbaran zone, NW Iran. Open J. Geol. 6, 859–874.
- Hedenquist, J.W., Arribas, A., Reynolds, T.J., 1998. Evolution of an intrusion centered hydrothermal system: Far Southeast-Lepanto porphyry and epithermal Cu–Au deposits, Philippines. Econ. Geol. 93, 373–404.
- Heinrich, C.A., 2005. The physical and chemical evolution of low-salinity magmatic fluids at the porphyry to epithermal transition: a thermodynamic study. Miner. Depos. 39, 864–889.
- Hoefs, J., 2004. Stable isotope geochemistry. Springer Verlag, Berlin, p. 244p.
 Hosseinzadeh, G.h., Calagari, A.A., Moayyed, M., Hadj Alilu, B., Moazzen, M., 2010.
 Study of hypogene alteration and copper mineralization in Sonajil area (East of Herris, East Azarbaidjan). J. Geosci. 74, 3–12 (in Persian with an English abstract).
- Jamali, H., Dilek, Y., Daliran, F., Yaghubpur, A., Mehrabi, B., 2010. Metallogeny and tectonic evolution of the Cenozoic Ahar- Arasbaran volcanic belt, northern Iran. Int. Geol. Rev. 53, 608–630.
- Jamali, H., Mahmoodabadipour, T., Shokohi, H., 2017. Geochemical halos of gold and associated elements in Nabijan gold index (SW Kaleibar, NW Iran). Petrol. 30, 139–156 (in Persian with an English abstract).
- Jannas, R.R., Beane, R.E., Ahler, B.A., Brosnahan, D.R., 1990. Gold and copper mineralization at the El Indio deposit, Chile. J. Geochem. Explor. 36, 233–266.
- Karimpour, M.H., Stern, C.R., Farmer, L., Saadat, S., Malekezadeh, A., 2011. Review of age, Rb–Sr geochemistry, and petrogenesis of Jurassic to Quaternary igneous rocks in Lut Block, Eastern Iran. Geopersia 1, 19–36.
- Komeili, S.S., Khalili, M., Asadi, H.H., Bagheri, H., Ayati, F., 2017. The nature of hydrothermal fluids in the Kahang porphyry copper deposit (Northeast of Isfahan) based on mineralography, fluid inclusion and stable isotope data. J. Econ. Geol. 8, 285–305.
- Konstantinov, M.M., Kryazhev, S.G., Ustinov, V.I., 2010. Characteristics of the oreforming system of the Zod gold-tellurium deposit (Armenia) according to isotopic data. Geochem. Int. 48, 946–949.
- Maghsoudi, A., Yazdi, M., Mehrpartou, M., Vosoughi, M., Younesi, S., 2014. Porphyry Cu–Au mineralization in the Mirkuh Ali Mirza magmatic complex, NW Iran. J. Asian Earth Sci. 79, 932–941.
- Mederer, J., Moritz, R., Zohrabyan, S., Vardanyan, A., Melkonyan, R., Ulianov, A., 2014.
 Base and precious metal mineralization in Middle Jurassic rocks of the Lesser Caucasus: a review of geology and metallogeny and new data from the Kapan, Alaverdi and Mehmana districts. Ore Geol. Rev. 58, 185–207.
- Mirnejad, H., Mathur, R., Hassanzadeh, J., Shafie, B., Nourali, S., 2013. Linking Cu mineralization to host porphyry emplacement: Re–Os ages of molybdenites versus U-Pb ages of zircons and sulfur isotope compositions of pyrite and chalcopyrite from the Iju and Sarkuh porphyry deposits in southeast Iran. Econ. Geol. 108, 861–870.
- Meinert, L.D., Hedenquist, J.W., Satoh, H., Matsuhisa, Y., 2003. Formation of anhydrous and hydrous skarn in Cu–Au ore deposits by magmatic fluids. Econ. Geol. 98, 147–156.
- Miranvari, A.S., Calagari, A.A., Ferdowsi, R., 2020. Evolution of ore-forming fluids in the Sarilar gold-bearing silicic veins: evidence from fluid inclusions and sulphur stable isotope studies, East Azarbaidjan, NW Iran. Period. di Mineral. 89, 265–278.
- Mollai, H., Sharma, R., Pe-Piper, G., 2009. Copper mineralization around the Ahar (NW Iran): evidence for evolution and the origin of the skarn ore deposit. Ore Geol. Rev. 35, 401–414.
- Moritz, R., Melkonyan, R., Selby, D., Popkhadze, N., Gugushvili, V., Tayan, R., Ramazanov, V., 2016a. Metallogeny of the Lesser Caucasus: From arc construction to post-collision evolution: in Richards, J., ed., Tethyan tectonics and metallogeny. Soc. Econ. Geol. Spec. Pub. 19, 157–192.
- Moritz, R., Rezeau, H., Ovtcharova, M., Tayan, R., Melkonyan, R., Hovakimyan, S., Ramazanov, V., Selby, D., Ulianov, A., Chiaradia, M., Putlitz, B., 2016b. Long-lived, stationary magmatism and pulsed porphyry systems during Tethyan subduction to post-collision evolution in the southernmost Lesser Caucasus, Armenia and Nakhitchevan. Gondwana Res. 37, 465–503.
- Nash, J.T., 1976. Fluid inclusion petrology, data from porphyry copper deposits and applications to exploration. United States Geology Survey Professional Paper 907-D, 1–16.
- Ohmoto, H., and Rye, R.O., 1979. Isotopes of sulfur and carbon: in Barnes, H.L., ed., Geochemistry of Hydrothermal Ore Deposits. New York, Wiley, 509–567.

- Omrani, J., Agard, P., Whitechurch, H., Benoit, M., Prouteau, G., Jolivet, L., 2008. Arc-magmatism and subduction history beneath the Zagros Mountain, Iran: a new report of adakites and geodynamic consequences. Lithos 106, 380–398.
- Radmard, K., Zamanian, H., Hosseinzadeh, M.R., Ahmadi Khalaji, A., 2017. Geochemistry and hydrothermal evolution of the Mazraeh Shadi-Hizehjan precious and base metal deposit, northeastern Tabriz, Iran. Neu. Jr. Mineral. Ab. 3, 227–250.
- Regional Company of Azerbaidjan Mines, 1995. Base and precious metals exploration project in Kharvana Region. Industries and Mines Organization of East-Azarbaidjan Province, 171 pp.
- Rezeau, H., Moritz, R., Wotzlaw, J.F., Tayan, R., Melkonyan, R., Ulianov, A., Selby, D., d'Abzac, F.X., Stern, R.A., 2016. Temporal and genetic link between incremental pluton assembly and pulsed porphyry Cu–Mo formation in accretionary orogens. Geol. 44, 627–630.
- Richards, J.P., 2015. Tectonic, magmatic, and metallogenic evolution of the Tethyan orogen: From subduction to collision. Ore Geol. Rev. 70, 323–345.
- Richards, J.P., Spell, T., Rameh, E., Razique, A., Fletcher, T., 2012. High Sr/Y magmas reflect arc maturity, high magmatic water content, and porphyry Cu \pm Mo \pm Au potential: examples from the Tethyan arcs of central and eastern Iran and western Pakistan. Econ. Geol. 107, 295–332.
- Richards, J.P., Wilkinson, D., Ullrich, T., 2006. Geology of the Sari Gunay epithermal gold deposit, northwest Iran. Econ. Geol. 101, 1455–1496.
- Robinson, B.W., Kusakabe, M., 1975. Quantitative preparation of sulfur dioxide for $^{34}\text{S}/^{32}\text{S}$ analyses from sulfides by combustion with cuprous oxide. Anal. Chem. 47, 1179–1181.
- Roedder, E., 1978. Silicate liquid immiscibility in magmas and in the system of K_2O -FeO-Al $_2O_3$ -SiO $_2$, an example of serendipity. Geochim. Cosmochim. Acta 42, 1597–1617.
- Roedder, E., 1984. Fluid Inclusions: Mineral. Soc. Am., Rev. Mineral. 12, 644 p.
- Rose, A.W., Burt, D.M., 1979. Hydrothermal alteration. In: Barnes, H.L. (Ed.), Geochemistry of hydrothermal ore deposits, 2nd ed.,. John Wiley and Sons, New York, p. 798 pp.
- Sakhdari, M., Yazdi, M., Behzadi, M., 2011. Geochemistry, Alteration and Mineralization of Gold in Shanegh Area, Delijan (Isfahan). J. Geosci. 81, 75–80 (in Persian with an English abstract).
- Seedorff, E., Dilles, J.H., Proffett, J.M., Einaudi, M.T., Zurcher, L., Stavast, W.J.A., Johnson, D.A., Barton, M., 2005. Porphyry deposits: Characteristics and origin of hypogene features. Econ. Geol. 100, 251–298.
- Sengör, A.M.C., Natal'in, B.A., 1996. Paleotectonics of Asia: fragments of a synthesis. In: Yin, A., Harrison, T.M. (Eds.), The tectonic evolution of Asia. Cambridge University Press, pp. 486–640.
- Shahabpour, J., 1982. Aspects of alteration and mineralization at the Sar-Cheshmeh copper–molybdenum deposit, Kerman, Iran. Dissertation, University of Leeds.
- Seward, T.M., Barnes, H.L., 1997. Metal transport by hydrothermal ore fluids. In: Barnes, H.L. (Ed.), Geochemistry of hydrothermal ore deposits. John Wiley and Sons, New York, pp. 435–486.
- Simmonds, V., 2013. Geochemistry and petrogenesis of an adaktic quartz-monzonitic porphyry stock and related cross-cutting dike suites, Kighal, northwest Iran. Int. Geol. Rev. 55, 1126–1144.
- Simmonds, V., 2019. Characteristics and timing of the Cu–Mo mineralization in the Kighal porphyry stock, NW Iran: Implications for the timing of porphyry Cu-related magmatism in Iran and southern Armenia. Ore Geol. Rev. 113, 103108.
- Simmonds, V., Calagari, A.A., Kyser, K., 2015. Fluid inclusion and stable isotope studies of the Kighal porphyry Cu–Mo prospect, East-Azarbaidjan, NW Iran. Arab. J. Geosci. 8, 437–453.
- Simmonds, V., Moazzen, M., 2015. Re–Os dating of molybdenites from Oligocene Cu–Mo–Au mineralized veins in the Qarachilar area, Qaradagh batholith (northwest Iran): Implications for understanding Cenozoic mineralization in South Armenia, Nakhchivan and Iran. Int. Geol. Rev. 57, 290–304.
- Simmonds, V., Moazzen, M., Harris, C., 2016. Stable isotopes (O, H and S) studies on the vein-type Cu–Mo–Au mineralization in Qarachilar area, Qaradagh pluton (NW Iran). Neu. Jb. Mineral. Ab. 193, 283–294.
- Simmonds, V., Moazzen, M., Mathur, R., 2017. Constraining the timing of porphyry mineralization in NW Iran in relation to Lesser Caucasus and Central Iran: Re–Os age data for Sungun porphyry Cu–Mo deposit. Int. Geol. Rev. 59, 1561–1574.
- Simmons, S.F., White, N.C., John, D.A., 2005. Geological characteristics of epithermal precious and base metal deposits. Econ. Geol. 100, 485–522.
- Singer, D.A., Berger, V.I., Menzie, W.D., Berger, B.B., 2005. Porphyry copper deposit density. Econ. Geol. 100, 491–514.
- Song, X., 1984. Minor elements and ore genesis of the Fankou lead–zinc deposit, China. Miner. Depos. 19, 95–104.
- Stampfli, G.M., 2000. In: Bozkhurt, E., Whichester, J.A., Piper, J.D.A. (Eds.), Tectonic and magmatism in Turkey and surrounding area, 173. Geol. Soc. London Spec. Pub, pp. 1–23.
- Taghipour, N., Aftabi, A., Mathur, R., 2008. Geology and Re–Os geochronology of mineralization of the Miduk porphyry copper deposit, Iran. Resour. Geol. 58, 143–160.
- Vernon, R.H., 2018. A practical guide to tock microstructure. Cambridge University Press.
- Whitney, D.L., Evans, B.W., 2010. Abbreviations for names of rock-forming minerals. Am. Mineral. 95, 185–187.
- Wilkinson, J.J., 2001. Fluid inclusion in hydrothermal ore deposits. Lithos 55, 229–272.Zvezdov, V.S., Migachev, I.F., Girfanov, M.M., 1993. Porphyry copper deposits of the CIS and the models of their formation. Ore Geol. Rev. 7, 511–549.